estec

European Space Research
and Technology Centre
Keplerlaan 1
2201 AZ Noordwijk
The Netherlands

T +31 (0)71 565 6565
F +31 (0)71 565 6040
www.esa.int

DOCUMENT

Sentinel-6 Michael Freilich POD Context

Page 1/48
Sentinel-6 Michael Freilich Precise Orbit Context
JC-TN-ESA-SY-0420
Date 03/05/2023
Issue 2 Rev 2

European Space Agency
Agence spatiale européenne

APPROVAL

Title Sentinel-6 Michael Freilich POD Context	
Issue 2	**Revision** 2
Author Robert Cullen ESA Sentinel-6 Payload System Manager	**Date** 03/05/2023 Digitally signed by Robert Cullen Date: 2023.05.04 17:09:43 +01'00'
Approved by	**Date** 03/05/2023
C. Maraldi (CNES)	Confirmed by email
R. Cullen (ESA)	Confirmed by email
Cristina Martin-Puig (EUMETSAT)	Confirmed by email
J-D Desjonqueres (NASA-JPL)	Confirmed by email
E. Leuliette (NOAA)	Confirmed by email

CHANGE LOG

Reason for change	Issue	Revision	Date
Major updated following review with track change	1	2	23/10/2020
Update of GNSS-POD DCM, GNSS-RO-POD patterns and Poseidon-4 reference information.	1	3	11/11/2020
End of Satellite in-orbit verification issue.	1	4	01/02/2021
Update to classification	1	5	21/07/2021
Update following commissioning	2	0	23/11/2021
Update following review	2	1	22/01/2022
Update for P4 in-orbit pointing assessment	2	2	01/12/2022

CHANGE RECORD

Issue 1	**Revision** 3		
Reason for change	**Date**	**Pages**	**Paragraph(s)**
§2.1.2 update of references	11/11/2020		§2.1.2
Link to Poseidon-4 antenna pattern cuts	19/11/2020	14	§3.5.1
Link to GNSS-RO-POD antenna patterns	19/11/2020	15	§3.5.2
Pre-launch AMR-C boresight vector	19/11/2020	15	§3.5.3
§5.3.4 updated GNSS-POD matrices based on RD5	11/11/2020	N/A	§5.3.4

Issue 1	**Revision** 4		
Reason for change	**Date**	**Pages**	**Paragraph(s)**

Update of the scope	01/02/2021	4	§1.1
§2.1.2 update of references	15/01/2021	5-6	§2.1.2
Mass properties updated	31/01/2021	9-10	§3.2.1
Poseidon-4 reference points updated	15/01/2021	14-17	§3.5.1
Updated AMR DCM	29/01/2021	18	§3.5.3
GNSS-POD description updated	01/02/2021	18-19	§3.5.4
Additional reference added for DORIS	29/01/2021	19	§3.5.5.1
Latest pre-launch star-tracker DCM	29/01/2021	21	§3.6
Other miscellaneous changes	01/02/2021	various	various

Issue 1	**Revision** 5		
Reason for change	**Date**	**Pages**	**Paragraph(s)**
Change of classification to releasable to public	20/07/2021	All	N/A

Issue 2	**Revision** 0		
Reason for change	**Date**	**Pages**	**Paragraph(s)**
Various cosmetic	23/11/2021	5, 16, 17, 26 and 28	N/A
Addition of 90° and 180° yaw bias	23/11/2021	10	§2.3
Satellite surfaces updated to 12 panel model with updated properties	23/11/2021	11-16	§2.4
Plots of DSP and SAP temperature at several solar beta angles	23/11/2021	15-16	§2.4.2.3.1
Updated list of manoeuvres	23/11/2021	27	§3.2

Issue 2	**Revision** 1		
Reason for change	**Date**	**Pages**	**Paragraph(s)**
Various cosmetic	22/01/2022	5	1.1
Satellite surfaces updated	22/01/2022	N/A	2.4
Updated list of manoeuvres	23/11/2021	27	§3.2

Issue 2	**Revision** 2 final		
Reason for change	**Date**	**Pages**	**Paragraph(s)**
Updated scope	03/04/2023	5	1.1
Acronyms	22/01/203	6	1.2
2.1 Reference frame information updated	04/04/2023	8	2.1
2.4.2.3 – clean up of text	04/04/2023	14	2.4.2.3
2.4.3 major update to describe pre and post launch analysis of pointing	03/05/2023	17-20	2.4.3

2.4.3.3 around the Y_p axis of about +0.0003° updated for the correct axis	03/05/2023	20	2.4.3.3
2.4.4 update to add information concerning GNSS-RO POD alignment	04/04/2023	21-22	2.4.4
2.4.4 Path for FTP added in hyperlink and footnote updated	03/05/2023	22	2.4.4
2.4.6.2 Path for FTP added in hyperlink and footnote updated	03/05/2023	22 around the Y_p axis of about +0.00034	2.4.6.2
2.5 Star tracker in-orbit alignment analysis added	04/04/2023	25-27	2.4.4
Updated list of 5 manoeuvres	01/05/2023	31	§3.2.3

Table of contents:

1 INTRODUCTION

1.1 Scope

This document provides all relevant Sentinel-6 Michael Freilich (S6-MF) parameters and information required to support Sentinel-6 precise orbit determination (POD) and other applications requiring metrology and alignment information of the platform and payload. This issue of the document has been updated based on the knowledge of the system at the end of the S6-MF commissioning phase.

All model inputs external to the satellite used in the POD process, for example, the constants for Earth parameters and non-gravitational forces are not within the scope of this document.

This document is provided with final photographs in §4.2 prior to satellite fuelling and encapsulation in the Falcon 9 launcher fairing. The main update relates to post-launch pointing information related to the Poseidon-4 radar altimeter antenna boresight pointing (§2.4.3), GNSS-RO POD antenna mounting information (§2.4.4) and star tracker alignment (§2.5) analysis information.

1.2 Acronyms and Abbreviations

AMR-C	Advanced Microwave Receiver (climate quality)
AOCS	Attitude and Orbit Control System
ARF	GNSS-POD Antenna Reference Frame (ARF)
ARP	GNSS-POD Antenna Reference Point (ARP)
BoL	Beginning of Life
BoS	Beginning of Science Mission
CCDB	Characterisation and Calibration Data Base
CESS	Course Earth Sun Sensor
CFRP	Carbon Fibre Reinforced Plastic
COG	Centre of Gravity
COM	Centre of Mass
DCM	Direct Cosine Matrix
DORIS	Doppler Orbitography and Radio positioning Integrated by Satellite
DSP	Deployable Solar Panel
EoL	End of Life
EoS	End of Science mission
GADS	Generic Auxiliary Data Specification
GNSS	Global Navigation Satellite System
GNSS-POD	GNSS unit used for primary navigation on-board
GNSS-RO	GNSS Radio Occultation
GNSS-RO-POD	GNSS Radio Occultation POD functionality
ICD	Interface Control Document
IR	Infra Red
LCL	Latch Current Limiter
LTAN	Local time at Ascending Node
LRA	Laser Retroreflector Array
MLI	Multi-Layer Insulation
MMFU	Mass memory functional unit
MPPS	Mono-Propellant Propulsion System
NAVATT	Navigation and attitude file. Output of the AOCS algorithm telemetered for use in the ground segment containing Kalman filtered quaternions and manoeuvre flags (ie., non nominal pointing modes of the satellite). Data ussed in NRT science data processing.
NRT	Near Real Time
OBC	On-board computer
P4	Poseidon-4 Radar altimeter
PD	Proposational Derivative
PCDU	Power Control and Distribution Unit

PID	Proportional Integral Derivative
PLM	Payload Module
POD	Precise Orbit Determination
PVA	Polyvinyl acetate
RCS	Reaction Control System
RF	Radio Frequency
RIU	Remote Interface Unit
RMU	Rate measurement unit
S6-MF	Sentinel-6 Michael Freilich
SA	Solar Array
SAP	Solar Array Power
SAR	Solar Array Regulator
SBM	Standby mode
SSM	Second surface mirrors
SRF	Satellite Reference Frame
VDA	Vacuum Deposited Aluminium

2 SATELLITE DESCRIPTION

The satellite configuration is summarised in below in Figure 2-1.

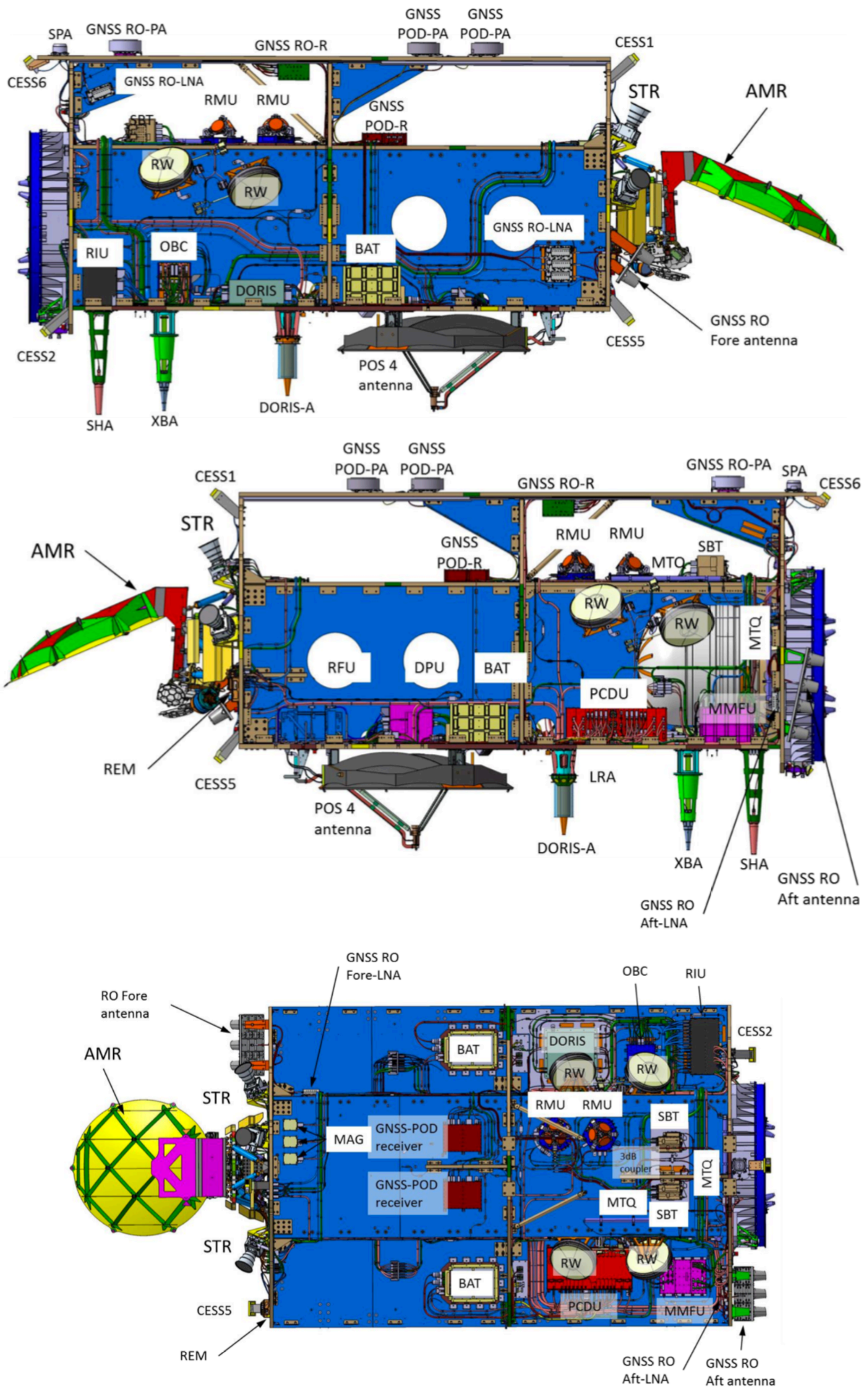

Figure 2-1 With reference to the definition of the spacecraft axes, Figure 2-2. (Top) Spacecraft looking along the +Y axis, (Middle) looking along the -Y axis and (Bottom) looking along the -Z axis.

2.1 Satellite and Piloting Reference Frame

The axes of the Satellite Reference Frame (SRF) is provided below in Figure 2-2.

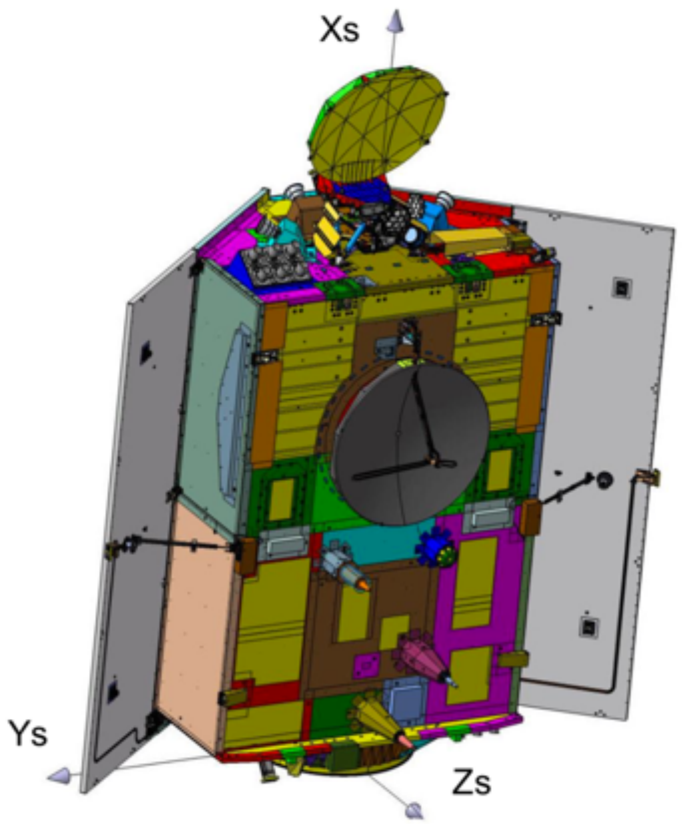

Figure 2-2 Satellite Reference frame definition origin is located at the interface plane separating the launcher and the satellite.

The SRF, $\overrightarrow{\mathbf{A_s}} = \{X_s, Y_s, Z_s\}$, is an orthogonal body-fixed axis system and it is designed to:

Origin S: The origin is located at the interface plane separating the launcher and the satellite, at the geometric centre of the launch adapter.

$+X_s$: is perpendicular to the Satellite/Launcher separation plane, pointing positively from the separation plane towards the Satellite, towards the flight direction parallel to the ground track

$+Z_s$: is pointing towards the satellite side, which is nominally earth pointing (Nadir), unless the Poseidon-4 electrical boresight is not parallel to Z_s (see below).

$+Y_s$: completes the right-handed orthogonal Spacecraft Reference Frame

In practice, the Poseidon-4 electrical boresight is not exactly parallel to Z_s and thus a Piloting frame $\overrightarrow{\mathbf{A_p}} = \{X_p, Y_p, Z_p\}$ is determined and the AOCS is configured to point Z_p anti-nadir to the local ellipsoidal normal and the X_p parallel to the instantaneous ground track vector (so called yaw steering).

2.2 Mass Properties

Satellite dry mass: 961.831 ± 0.24 kg as measured with accuracy of 0.1% during mass properties test with a wet mass of 1191.831 kg.

The Centre of Mass (CoM) rounded to the nearest mm, in the Spacecraft Reference Frame at BoL with 0 kg (dry) propellant and solar arrays deployed is given by

$$r_{COM\_dry} = \begin{bmatrix} 1734.0 \\ -9.0 \\ 46.0 \end{bmatrix} \begin{bmatrix} X_s \\ Y_s \\ Z_s \end{bmatrix} \quad \text{mm}$$

The CoM at BoL with 230 kg (wet) of propellant and with solar arrays deployed, rounded to the nearest mm is

$$r_{COM\_wet} = \begin{bmatrix} 1527.0 \\ -7.0 \\ 37.0 \end{bmatrix} \begin{bmatrix} X_s \\ Y_s \\ Z_s \end{bmatrix} \quad \text{mm}$$

The CoM at the Beginning of Science (BoS) with an assumed 209 kg (wet) mass and having assumed a conservative 21 kg acquiring the reference orbit then, rounded to the nearest mm, the CoM position is

$$r_{COM_{wet-BoS}} = \begin{bmatrix} 1538.0 \\ -8.0 \\ 38.0 \end{bmatrix} \begin{bmatrix} X_s \\ Y_s \\ Z_s \end{bmatrix}$$

The CoM at the End of Science (EoS) rounded to the nearest mm, with an assumed 197 kg (wet) mass after having assumed 12 kg depleted for collision avoidance and maintenance manoeuvres is

$$r_{COM_{wet-EoS}} = \begin{bmatrix} 1545.0 \\ -8.0 \\ 38.0 \end{bmatrix} \begin{bmatrix} X_s \\ Y_s \\ Z_s \end{bmatrix}$$

The area perpendicular to the satellite flight direction is 4,091655 m^2.
This corresponds to an area per mass of 0.00425 m^2/kg dry and 0,00343 m^2/kg wet (BoL).

2.2.1 Centre of mass position and knowledge during science operations phase

The analysed CoM position with associated uncertainty is provided in the following table. Note unlike in the last sub-section, these values are not rounded to the nearest mm.

Jason-CS / Sentinel-6 (Industry predictions)	**Beginning of Life**	**End of scientific mission**	**Accuracy**
Satellite Mass	1191.831 kg	1158.531 kg	0.1%
X coordinate of the satellite CoM	1527.4 mm	1545.2 mm	± 1.2 mm
Y coordinate of the satellite CoM	-7.325 mm	-7.52 mm	± 0.8 mm
Z coordinate of the satellite CoM	37.341 mm	38.414 mm	± 0.8 mm

Table 4.2.2 Sentinel-6A Satellite Mass Properties

CoM determination through mission lifetime
During operations, the mass file provided by EUMETSAT with the filetype 'AX____SMR__AX' can be used, contains the respective propellant mass and COM location.
For example, from the file
'S6A_AX____SMR__AX_20201216T090329_20201216T090329_20201216T092737_________________MOC__OPE_AL____.SEN6'

The following parameters are retrieved:

```
S6A MASS PROPERTIES COMPUTED ON 2020-12-16T09:03:29
 2020-12-16T09:03:29 CALCULATION DATE
  1.533 XS CO-ORDINATE (METER)
 -0.007 YS CO-ORDINATE (METER)
```

```
  0.037 ZS CO-ORDINATE (METER)
 1180.633 TOTAL S/C MASS (KG)
 218.530 FUEL MASS (KG)
   697.0 INERTIA XX (M2.KG)
  1808.5 INERTIA YY (M2.KG)
  2068.3 INERTIA ZZ (M2.KG)
     6.7 INERTIA XY (M2.KG)
    -2.1 INERTIA YZ (M2.KG)
    16.1 INERTIA ZX (M2.KG)
```

It can be seen that at the assumed beginning of operations following acquisition of the reference orbit (last manoeuvre completed 2020-12-18T00:40:31.997940 UTC)

$$r_{COM_{ref}} = \begin{bmatrix} 1533.0 \\ -7.0 \\ 37.0 \end{bmatrix} \begin{bmatrix} X_s \\ Y_s \\ Z_s \end{bmatrix} \text{mm}$$

2.3 Attitude control

The attitude control of the satellite is provided by the Attitude and Orbit Control System (AOCS) and is based on five main operational modes.
The key mode during science operations is the Normal Mode termed AOC-NOM. During AOC-NOM the attitude is controlled by means of GNSS-POD and Star trackers as sensing elements and with reaction wheels as actuators. Magnetic torquers are used for continuous wheel off-loading. A robust proportional-derivative (PD) control law provides 3-axis local normal pointing attitude control. In addition, a position-dependant rotation around the Nadir axis ("yaw steering") is performed in order to align the satellite X_S axis with the velocity vector relative to the Earth surface in order to ease altimeter payload measurement processing. During commissioning it is possible the satellite might also be orientated with its x-axis parallel with the anti-velocity vector relative to earth surface, i.e., 180° to the nominal direction.
There are three science calibration manoeuvres:

1. the AMR-C calibration manoeuvres around the satellite pitch axis, are performed by commanding dedicated pointing biases, see §3.2.1.
2. The Poseidon-4 altimeter manoeuvre rotates the satellite in pitch and roll by up to ±0.4° with various combinations, and with yaw bias of ±90°, see §3.2.2.
3. 180° yaw bias manoeuvres over ~4 days about 0° solar beta angles to support POD, see §3.2.3.

For completeness, the four other modes are:
Standby Mode (AOC-SBM) is an initial AOCS mode introduced to support ground testing.

Acquisition and Safe Mode (AOC-ASM)
The AOC-ASM phase can be broken down into four sub-modes. Rate damping is the first phase after launcher separation. The satellite may have any attitude and an angular rate up to 2.5 deg/s. The rate damping is performed by the Rate Measurement Unit (RMU) and the thrusters, decreasing the angular rate to 0.3 Deg/s.
After the initial rate damping, the solar array is being deployed. During the solar array deployment process, no active AOCS control is performed. Once the solar array has been completely deployed, the rate damping mode is re-entered even though no significant rate build-up is to be expected for Sentinel-6 satellites.
After solar array deployment and when the rate is below 0.3deg/s, the Coarse Earth and Sun Sensor (CESS) acquires the earth and sun vector. The Reaction Control System (RCS) then aligns the spacecraft pointing direction with Nadir, providing a coarse accuracy of better than 25°.
The last step within the Acquisition and Safe Mode is the yaw acquisition. It is done by processing of CESS and RMU data and using the RCS and the magnetic torquers for an alignment of the x-axis with flight direction, placing the solar array and the radiators in operable positions. This mode is also entered during satellite safe modes, of course omitting the solar array deployment phase.

Orbit Control Mode (AOC-OCM)
For orbit maintenance the Orbit Control Mode is used. After an initial attitude acquisition, slews can be commanded to the targeted thruster firing position by means of reaction wheels and the spacecraft attitude is stabilised until the Δv manoeuvre starts. The in- or out-of-plane Δv manoeuvre is performed and subsequently the nominal spacecraft attitude restored by a slew.

2.4 Satellite surfaces

This issue of the document provides a 12 panel characterisation for which it is left to the reader to establish how to use the properties and characterisation for their POD application. It is also noted that the reader can refer to the drawings shown in §4 as to establishing a different model for the application.

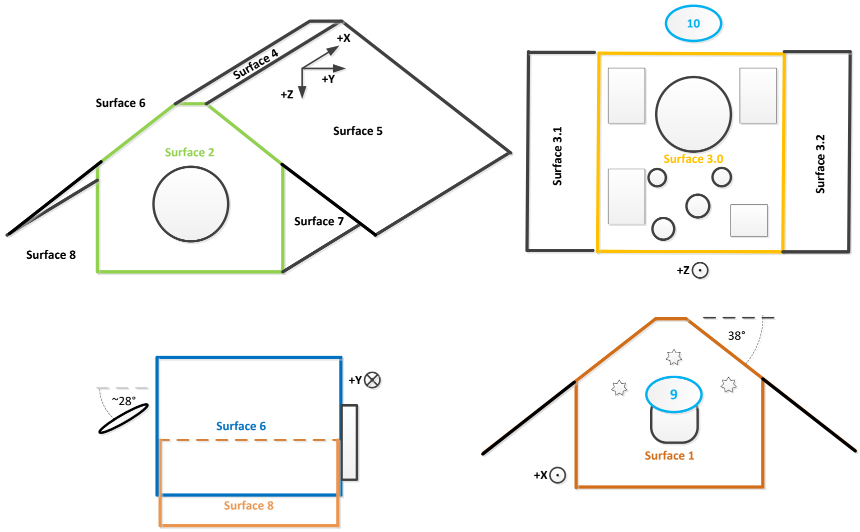

Figure 2-3 The 12 panel model for which properties are provided in §2.4.1

2.4.1 Thermo-optical properties

The satellite configuration includes 12 surface areas as shown in Table 2-1. The given orientations of the satellite refer to the coordinates of the vector normal to the surface and are oriented from inside to outside with respect to the SRF. The given property values are weighted with their fraction of the total surface area. This can be a mixture of Kapton, Single Surface Mirrors (SSM), white paint, etc.

Surface Orientation	1 PX	2 MX	3.0 PZ	3.1 PY	3.2 MY	4 MZ	5 PYMZ	6 MYMZ	7 PY	8 MY	9 PXMZ	10 PXPZ	
Remark	w/o AMR-C		Nadir panels	DSP Rear Side (38°)	DSP Rear Side (38°)	Zenith panel w/o SAP and DSP	SAP and DSP (38°)	SAP and DSP (38°)	Closure panels w/o SAP and DSP	Closure panels w/o SAP and DSP	AMR Back (~28° tilted)	AMR Reflector (~28° tilted)	
Area [m²]	2.99	3.35	9.03	4.09	4.09	1.80	8.65	8.65	2.87	2.87	0.92	0.92	
Surface material	MLI	MLI	SSM, MLI & POS4 Sunshield	CFRP	CFRP	SSM & MLI	CFRP & PV	CFRP & PV	MLI	MLI	Black SLI	Reflector Coating	
Refl. Spec	**0.50**	**0.50**	**0.60**	**0.00**	**0.00**	**0.65**	**0.00**	**0.00**	**0.50**	**0.50**	**0.00**	**0.19**	**BOL**
Refl. Diff	**0.04**	**0.04**	**0.02**	**0.16**	**0.16**	**0.03**	**0.14**	**0.14**	**0.04**	**0.04**	**0.08**	**0.56**	
Absorptivity (	**0.46**	**0.46**	**0.37**	**0.84**	**0.84**	**0.33**	**0.86**	**0.86**	**0.46**	**0.46**	**0.92**	**0.25**	
Refl. Spec	**0.38**	**0.38**	**0.50**	**0.00**	**0.00**	**0.55**	**0.00**	**0.00**	**0.38**	**0.38**	**0.00**	**0.15**	**EOL**
Refl. Diff	**0.04**	**0.04**	**0.02**	**0.16**	**0.16**	**0.03**	**0.13**	**0.13**	**0.04**	**0.04**	**0.08**	**0.45**	
Absorptivity (	**0.58**	**0.58**	**0.48**	**0.84**	**0.84**	**0.42**	**0.87**	**0.87**	**0.58**	**0.58**	**0.92**	**0.40**	
Refl. Spec	**0.21**	**0.21**	**0.20**	**0.00**	**0.00**	**0.23**	**0.00**	**0.00**	**0.21**	**0.21**	**0.00**	**0.00**	**BOL/EOL**
Refl. Diff	**0.02**	**0.02**	**0.06**	**0.20**	**0.20**	**0.01**	**0.20**	**0.20**	**0.02**	**0.02**	**0.12**	**0.75**	
Emissivity (IR	**0.77**	**0.77**	**0.75**	**0.80**	**0.80**	**0.76**	**0.80**	**0.80**	**0.77**	**0.77**	**0.88**	**0.25**	

Table 2-1 Sentinel-6 MF satellite surface properties (ultraviolet) with respect to the 12 panels shown in Figure 2-3.

Radiator	Area (m²)	Approximate dimensions (mm)	Areal margin (%)
Poseidon-4 (RFU and DPU)	1.244	3 areas	47
GNSS-RO-E	0.712	1423 x 500	10
Battery	0.053 each	230 x 230	8
PCDU	0.225	682 x 330	67
MMFU	0.135	410 x 330	67
X-Band	0.151	2 areas	50
DORIS	0.345	550 x 680	29
OBC	0.120	273 x 440	50
RIU	0.266	450 x 550	50

Table 2-2 Radiator sizes with remaining areal design margin (not required for POD)

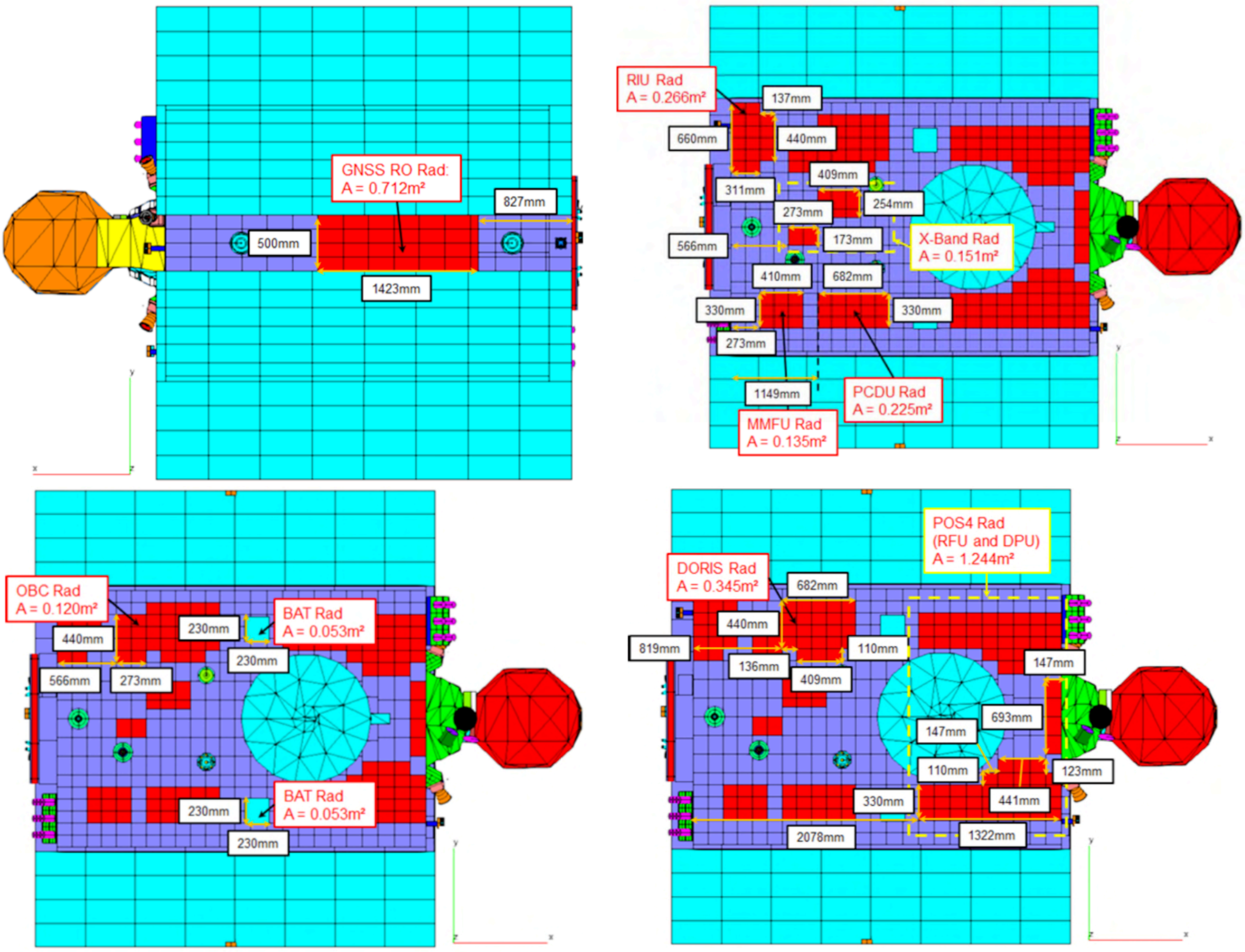

Table 2-3 (Top left) Radiators on the zenith panel shown in red. (Top right and bottom) Radiators on the nadir panel shown in Red. The four images indicate all radiators.

2.4.2 *Additional information for surface forces modelling*

The following information supports surface forces modelling (radiation pressure including thermal effects and drag).

2.4.2.1 Solar panels and dimensions

Each panel is a sandwich made of aluminium honeycomb (3/16”) covered by carbon fibre face sheets (5 layers). The layup is orthotropic in order to provide stiffness distribution compliant to solar array stiffness requirements (more stiffness in the long side of the panels). The front face sheet is covered by a 50 μ m Kapton foil to provide insulation against the electrical PVA laydown. The honeycomb edges are covered by Kapton tape, perforated in order to allow for venting during lift-off. The panel rear side is uncoated CFRP face sheet.
The Solar Array Panel (SAP) and Deployable Solar Panel (DSP) substrate areas are:

- SAP: 3681 mm x 1249 mm x 40 mm, 4.60 m²
- DSP: 3681 mm x 1122 mm x 40 mm, 4.13 m².

Hence, once the DSPs are deployed the full solar array area is SAP+DSP. The dimensions are provided in Figure 2-4.

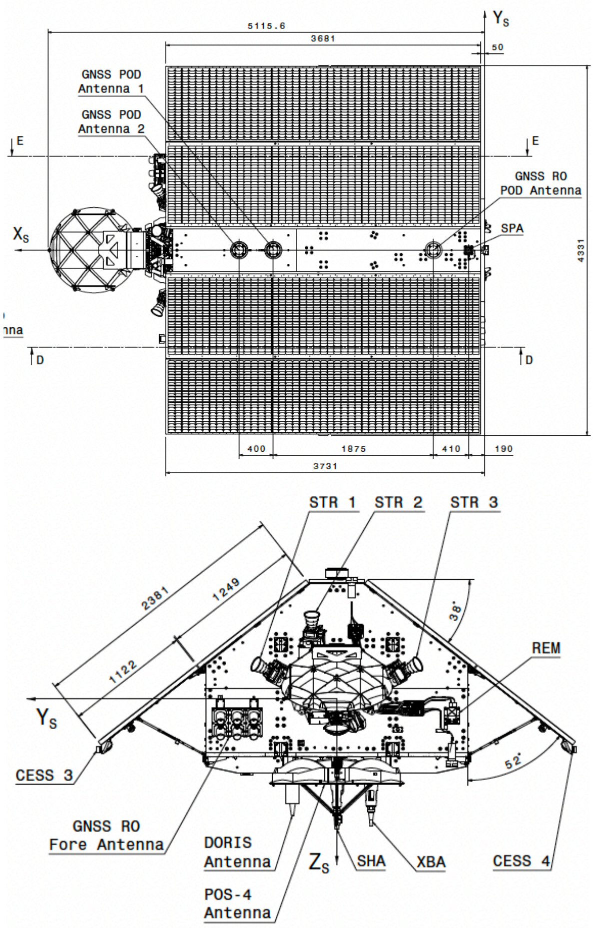

Figure 2-4 Deployed solar array area.

2.4.2.2 Solar panels efficiency

Concerning electric balance of the solar array and efficiency): As a reference, the panel output power under standardised conditions at BoL, at AM0 (1367 W/cm2[1]), 28° C and at Pmax are: 1443 W from Solar Array Power (SAP), 1337 W from Deployable Solar Panel (DSP) at the solar array interface. The worst-case real SA power under flight conditions has been calculated by industry for a complete Senintel-6 orbit, LTAN 06:00h, summer solstice, consideration of temperature cycle, including one string loss, including all loss factors with a global loss of 0.95, and at EOL.

The average power over this orbit is 1025 W assuming that the SA is always operated at its maximum power point. This satisfies the system requirement of 1005 W orbit average power.
The efficiency of each Solar Array Regulator (SAR) varies with battery voltage and solar array voltage over satellite lifetime.

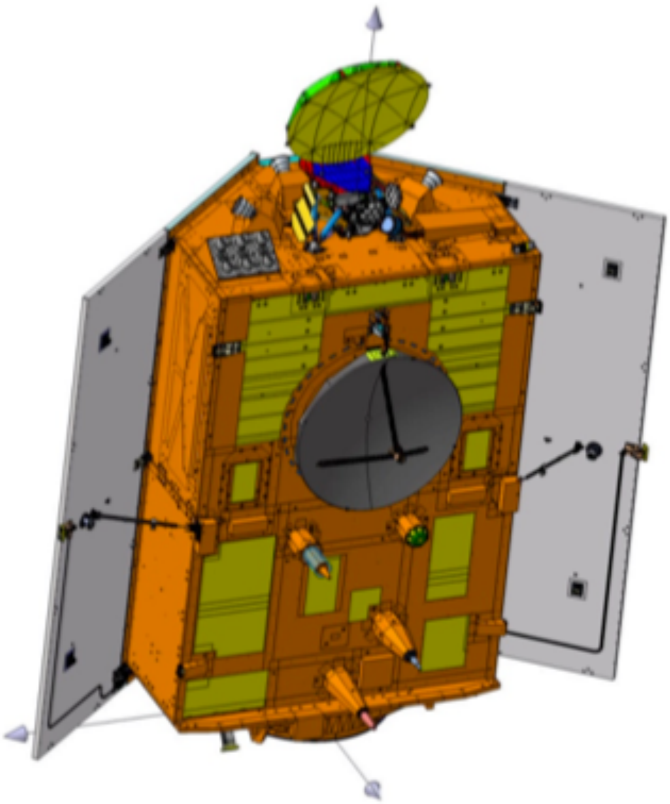

Figure 2-5 MLI covering in orange, SSM in yellow and CFRP in grey.

2.4.2.3 Thermal flows

The Poseidon-4 altimeter is located on the nadir pointing Payload Module (PLM) which is made from aluminium honeycomb. Thermally, the PLM main panel is separated from the main structure by means of titanium washers. The dissipated heat of the Radar Altimeter electronics is conducted to the radiating areas on the panels on ±Y-axis of the radar altimeter antenna. SSM covered surfaces radiate the heat towards Nadir. Heat pipes are embedded in the panel for effective conduction of the dissipated heat from the location behind the antenna to the radiator areas and enhance

[1] the standard tests for a solar array are given in the condition of Air Mass 0 (AM0). The Earth receives on average ~1350 w/m² of energy at winter solstice.

the temperature distribution across the PLM main panel. The Radar Altimeter antenna is mounted to the instrument platform by isostatic mounts. In order to avoid sun trapping between antenna and instrument platform a curtain of Multi-Layer Insulation (MLI) is mounted between the antenna rim and instrument platform."

The AMR-C thermal design is defined by NASA-JPL. At the system level the interface is formed by the PLM Front Panel. The instrument is thermally de-coupled by low conductive struts and MLI on the front panel as well as the radiometer. The PCDU provides main and redundant Latch Current Limiters (LCL) for thermal control. As the AMR-C requires a Proportional Integral Derivative (PID) temperature control (for stability reasons) which the Sentinel-6 PCDU cannot provide, a dedicated thermal control algorithm using Pulse Width Modulation is developed and provided by NASA-JPL. The two dedicated radiator plates of the AMR-C are located on ±Y side of the antenna feed and are rejecting the waste heat, unlike the majority of the units, not to nadir but normal to the orbital plane.

The **Solar Array** is thermally de-coupled from the satellite structure. Additionally, two deployable panels will unfold on ±Y side to extend the useable area. The composite contains a single layer Vacuum Deposited Aluminium (VDA) in order to increase the heat exchange between the two spacecraft sides of the body mounted panels. The deployable panels remain uncoated on their back and can therefore absorb Earth infrared (IR).

2.4.2.3.1 In-orbit solar and deployable panel thermal behaviour

SAP and DSP thermal behaviour characteristics are provided in Figure 2-6 for five solar-beta angle representative cases (approximately -80°, -45°, 0°, +45° and +80°) for Sentinel-6 MF. Thermistors are mounted on the surfaces with solar cells.

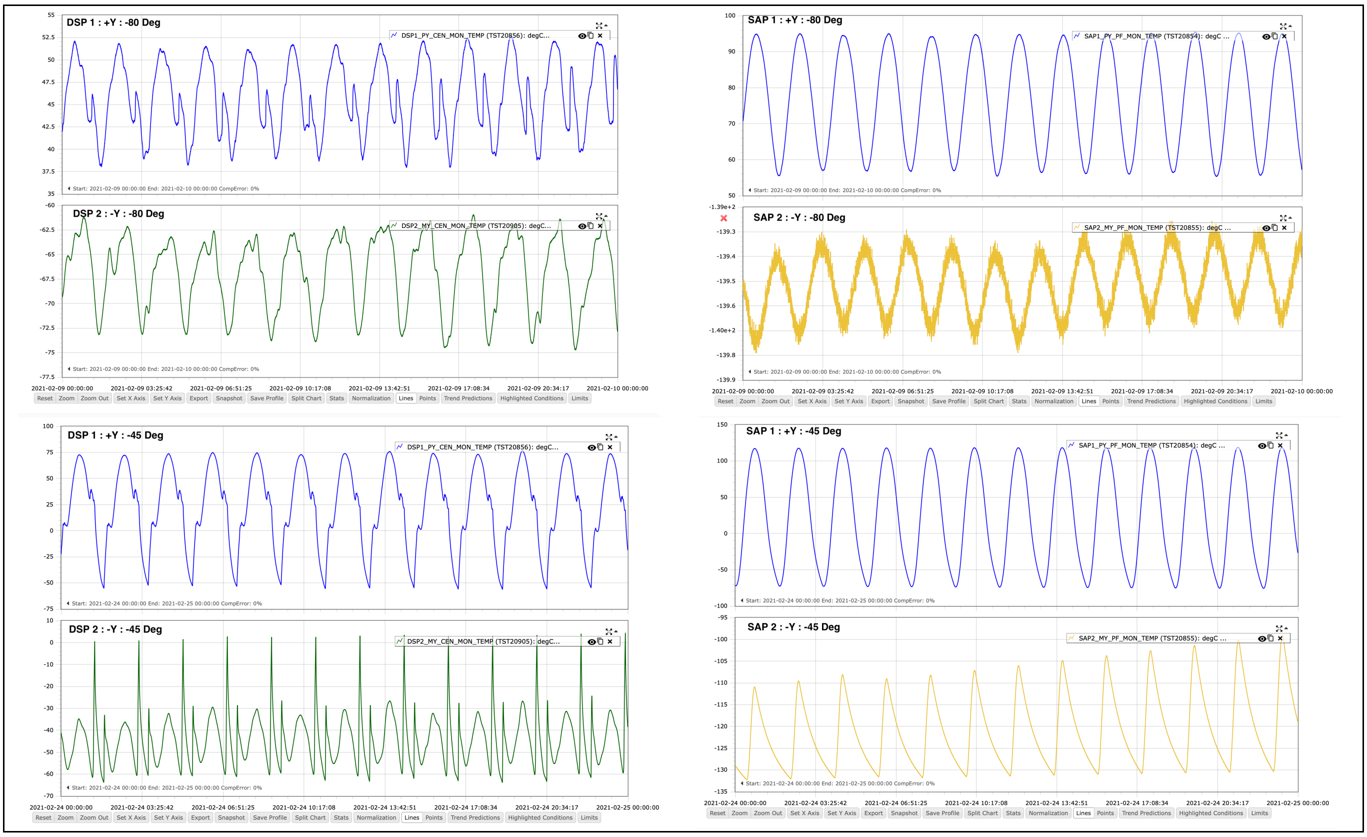

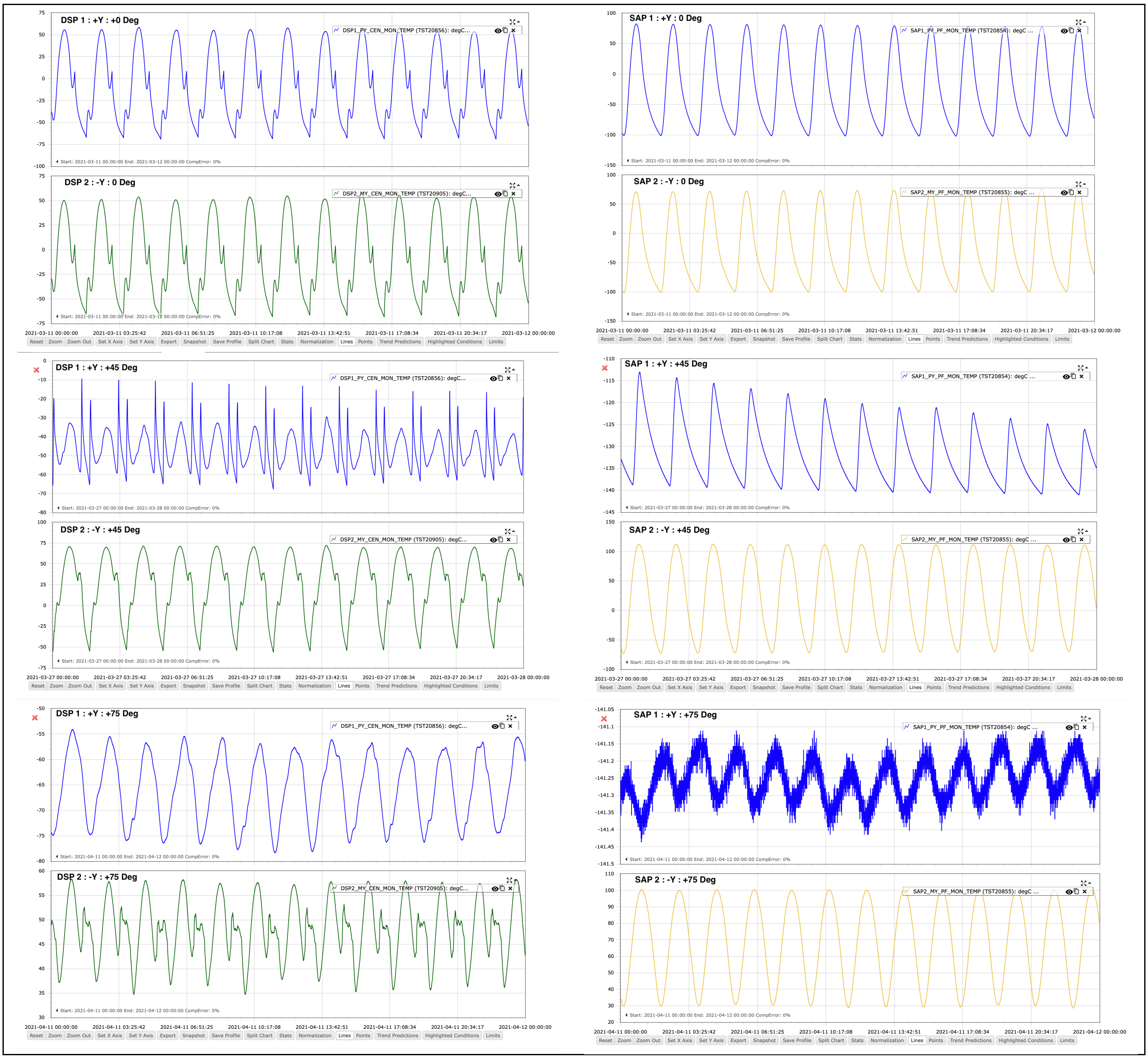

Figure 2-6 DSP (Left) and SAP (Right) thermistor plots at (from top to bottom) approximately -80°,-45°, 0°, +45° and +75° of solar beta angle. Each of the 12 plots shows the DSP or SAP elements pointing in the +Y (top denoted 1) and -Y (bottom denoted 2).

Reference points

This section provides the key reference points as measured during metrology and alignment during the environmental testing.

2.4.3 *Poseidon-4 Electrical Boresight Pointing*

The system is designed such that the estimated Poseidon-4 electrical boresight vector, $\vec{r}_{P4\_boresight}$, is pointed anti nadir to the local ellipsoidal normal.
Since the system is not perfect, i.e., the electrical boresight is not parallel to the mechanical boresight and the installation of the radar altimeter panel on the satellite is imperfect, then in-orbit the satellite AOCS is configured to slightly rotate and point the estimated electrical boresight anti nadir to the local ellipsoidal by means of the Piloting frame $\overrightarrow{\mathbf{A_p}}$, see §2.1.
This also is not perfect, in the sense that during the launch sequence the satellite experiences vibration, acoustic and shock interference that can result in the on-ground characterisation requiring in-orbit tuning, if performances are degraded, but normally can be handled in processing once pointing biases are known.
There are three elements to consider:

1. The pre-launch configuration of the AOCS based on the on-ground alignment characterisation of the system;
2. Post-launch re-configuration, if any. To date there has been no re-configuration of the S6-MF AOCS (see §2.5.1, though relative biases between the three star trackers have been assessed and shown to be within requirement);
3. Post launch end to end system tests over ocean to establish pointing biases that need to be communicated to the User community.

2.4.3.1 Poseidon-4 on-ground characterisation

The following establishes the on-ground measured electrical boresight vector within the SRF.

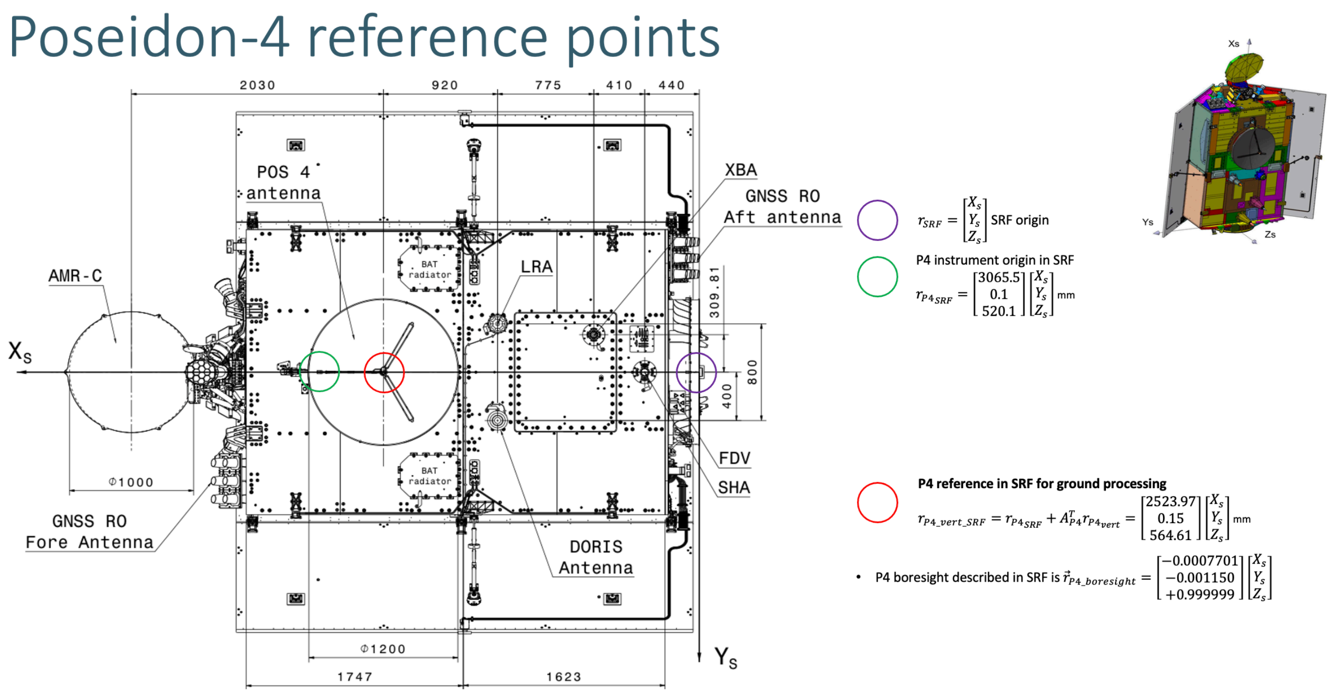

Figure 2-7 The Satellite Reference Frame definition with the key reference points of the Poseidon-4 viewing from underneath the satellite.

The transformation from the spacecraft reference to the altimeter reference frame is described by the following direction cosine matrix (DCM) below, which by designis a unitary matrix:

$$A_{P4} = \begin{bmatrix} 0.99999973 & -0.00000042 & 0.00072905 \\ -0.00000042 & 0.99999935 & 0.00114184 \\ -0.00072905 & -0.00114184 & 0.99999908 \end{bmatrix}$$

This corresponds to a rotation around the spacecraft X axis (roll) of approximately +0.0654°and around the spacecraft Y axis (pitch) of about -0.04177° and a negligible Z axis (yaw) of 23.85μ°.

The AOCS is configured such that the following Piloting frame $\overrightarrow{\mathbf{A_p}}$, see §2.1, is determined and uploaded to the satellite

In other words,

$$\overrightarrow{\mathbf{A_p}} = A_{P4}\overrightarrow{\mathbf{A_s}}.$$

The AOCS is configured to rotate $\overrightarrow{\mathbf{A_p}}$ such that to point Z_p anti-nadir to the local ellipsoidal normal and the X_p parallel to the instantaneous ground track vector (so called yaw steering).

The Poseidon instrument Reference Frame (termed RAA) is an orthogonal body-fixed axis system whose origin in the satellite reference frame is the following

$$r_{P4\_SRF} = \begin{bmatrix} 3065.5 \\ 0.1 \\ 520.1 \end{bmatrix} \begin{bmatrix} X_s \\ Y_s \\ Z_s \end{bmatrix} \text{mm}$$

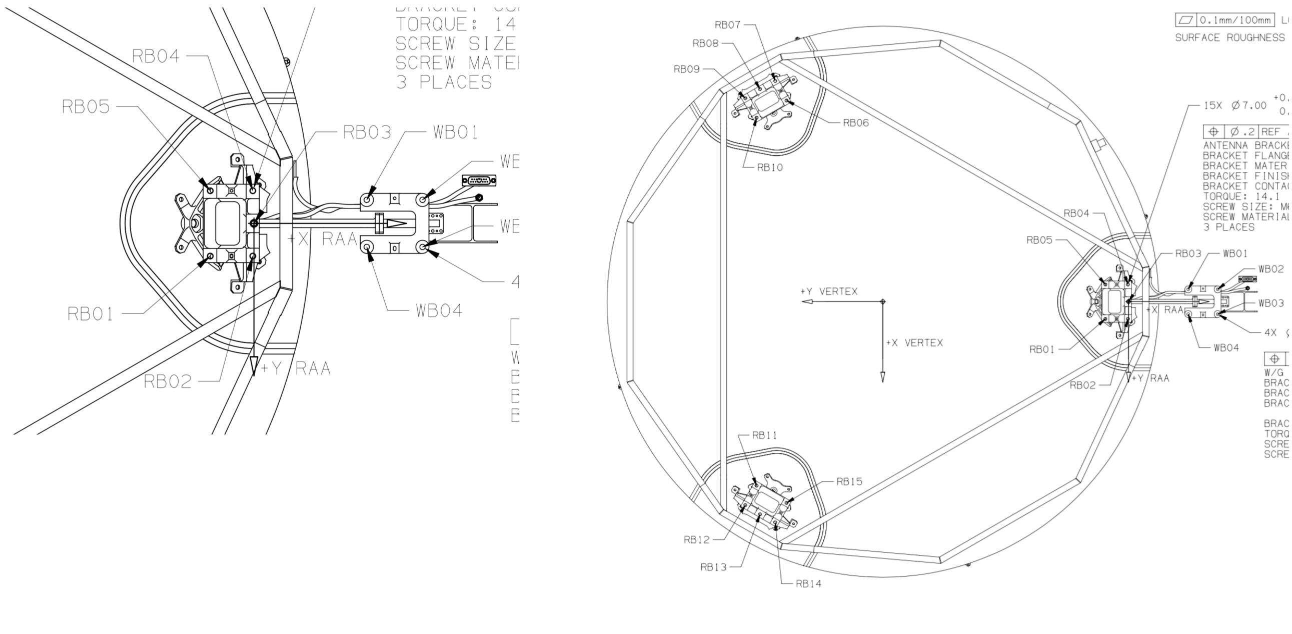

Figure 2-8 (Left) Poseidon-4 instrument reference (RAA) frame definition , which is by design orthogonal with the satellite reference frame (see Figure 2-7), though in practice has a small rotation since physically it is linked with the assembly of an instrument panel onto the satellite structure. (Right) RF measurements have been defined in an antenna reference (vertex) frame for RF measurements, though all analysed measurements provided in this section have been translated from this frame to the RAA and the SRF.

The normalised boresight vector of the P4 in the SRF is given by:

$$\vec{r}_{P4\_boresight} = \begin{bmatrix} -0.0007701 \\ -0.001150 \\ +0.999999 \end{bmatrix} \begin{bmatrix} X_s \\ Y_s \\ Z_s \end{bmatrix}$$

It is this vector that is configured in orbit to point anti-normal to the ellipsoid at any given time.

2.4.3.2 Poseidon-4 reference point for ground processing

The Poseidon-4 RF reference point described in the instrument reference frame (termed RAA)

$$r_{P4\_ref} = \begin{bmatrix} -541.5 \\ 0.1 \\ 44.9 \end{bmatrix} \begin{bmatrix} X_{RAA} \\ Y_{RAA} \\ Z_{RAA} \end{bmatrix} \text{mm}$$

The Poseidon-4 RF reference point for use in on-ground processing, as described in the SRF is given by

$$r_{P4\_vert\_SRF} = r_{P4} + A_{P4}^T r_{P4\_ref}$$

Where, $A_{P4}^T$is the transpose of A_{P4}.

$$r_{P4\_vert\_SRF} = \begin{bmatrix} 2523.97 \\ 0.15 \\ 564.61 \end{bmatrix} \begin{bmatrix} X_s \\ Y_s \\ Z_s \end{bmatrix} \text{mm}$$

2.4.3.3 On-Ground Characterisation and configuration derived from in-orbit operations

Based on along-track in-orbit Poseidon-4 stack processing analysis[2] of nominal and ±90° yaw steered pointing experiments (see §3.2), it has been demonstrated there is a still a residual bias in the nominal pointing of $\vec{r}_{P4\_boresight}$ with respect to anti local normal to the ellipsoid. In other words, the piloting frame $\{X_p, Y_p, Z_p\}$ is not perfectly tuned for nominal pointing. This is either due to on-ground alignment measurement, or most likely the impacts of acoustic, vibration and shock loads during the launch sequence of the satellite.

The use of the stack processing is accurate to few milli degrees and the electrical boresight of the Poseidon-4 was found to differ from the nominal configuration made pre-launch, i.e., $\overrightarrow{\mathbf{A_p}}$.

The analysis indicates to a rotation around the piloting spacecraft:

- X_p axis of approximately -0.031°and
- around the Y_p axis of about +0.0003°.

This corresponds to an effective roll and pitch of the piloting reference frame that would be required to correct the overall spacecraft pointing to become nominal.

It is required these angles are communicated to Users of the S6 data products.

[2] Scagliola, M., Fornari, M., Tagliani, N., Pitch Estimation for CryoSat by Analysis of Stacks of Single-Look Echoes, IEEE Geosci. And Remote Sens. Letter. Vol. 12 , Issue 7 , July 2015, doi: 10.1109/LGRS.2015.2413135.

At the time of writing, no further tuning of the AOCS pointing configuration is required since system performance requirements are met with respect to pointing. If the occasion arise that the AOCS is reconfigured, i.e.,an updated $\overrightarrow{\mathbf{A_p}}$ is determined and uploaded to the satellite, then this document (section §2.4.3) will be updated to reflect the new piloting frame and that the angles described above will essentially become zero.

2.4.4 GNSS-RO front, rear and POD antenna normal and position vectors

The front GNSS-RO antenna sub-system is mounted at the front of the satellite (also termed fore) approximately in the +X axis (see Figure 2-1 and Figure 2-2) though dipped in the +Z axis by about 34°. The rear antenna sub-system (also termed aft) is mounted at the back of the satellite approximately pointing in the -X axis direction and slightly dipped in the +Z axis by about 12°.
The normal vectors for each of the GNSS-RO reference frame plane (front and rear antenna units) is given by the following direction vectors.

$$\vec{r}_{RO-Front} = \begin{bmatrix} 0.829299490 \\ -0.000146952 \\ 0.558804379 \end{bmatrix} \begin{bmatrix} X_s \\ Y_s \\ Z_s \end{bmatrix}$$

$$\vec{r}_{RO-Rear} = \begin{bmatrix} -0.978107674 \\ -0.000388750 \\ 0.208099082 \end{bmatrix} \begin{bmatrix} X_s \\ Y_s \\ Z_s \end{bmatrix}$$

The antenna plane inclination with respect to the satellite reference frame for the front and rear antenna units are

Plane inclination angle	Measured (°)
GNSS-RO front antenna	33.973
GNSS-RO rear antenna	12.011

Table 2-4 GNSS-RO antenna plane inclination angles.

The GNSS-RO antenna (front, rear and roof POD) reference frame origins (not phase centre) described in the SRF are given by

$$r_{RO-Front} = \begin{bmatrix} 3727.256 \\ 730.614 \\ 293.333 \end{bmatrix} \begin{bmatrix} X_s \\ Y_s \\ Z_s \end{bmatrix} \qquad \text{mm}$$

$$r_{RO-Rear} = \begin{bmatrix} 210.176 \\ -792.758 \\ 421.376 \end{bmatrix} \begin{bmatrix} X_s \\ Y_s \\ Z_s \end{bmatrix} \qquad \text{mm}$$

$$r_{RO-POD} = \begin{bmatrix} 599.952 \\ -0.408 \\ -1095.055 \end{bmatrix} \begin{bmatrix} X_s \\ Y_s \\ Z_s \end{bmatrix} \qquad \text{mm}$$

The DCM matrices transferring from SRF to each of the front, rear and POD antenna reference frames, are:

$$A_{RO-Front} = \begin{bmatrix} 0.000018156 & -0.999999958 & -0.000289921 \\ 0.558804398 & 0.000250577 & -0.829299452 \\ 0.829299490 & -0.000146952 & 0.5588043791 \end{bmatrix}$$

$$A_{RO-Rear} = \begin{bmatrix} -0.000372889 & 0.999999924 & 0.000115445 \\ -0.208099111 & 0.000035320 & -0.978107744 \\ -0.978107674 & -0.000388750 & 0.208099082 \end{bmatrix}$$

$$A_{RO-POD} = \begin{bmatrix} 0.999998870 & -0.001201048 & 0.000904597 \\ -0.001201039 & -0.999999279 & -0.000009935 \\ 0.000904608 & 0.000008849 & -0.999999591 \end{bmatrix}$$

Antenna phase centres for the GNSS-RO are not available for inclusion into this document. Phase centres for the different GPS signals most likely differ.

The patterns for the GNSS-RO-POD antenna can be found here[3]. Model 47 corresponds to the Sentinel-6 MF antenna pattern and 48 for Sentinel-6 B.

2.4.4.1 Some notes concerning accommodation of the GNSS-RO POD antenna

The GNSS-RO POD antenna positioning information provided above is not the phase centre of the antenna. By agreement between ESA and NASA-JPL the position vector, r_{RO-POD} is the average of four mounting interface points as shown in Figure 2-9,
Detailed analysis of measurement values, see Table 2-5 show that antenna baseplate is slightly rotated (-0,07°) around the Z-axis of the antenna.

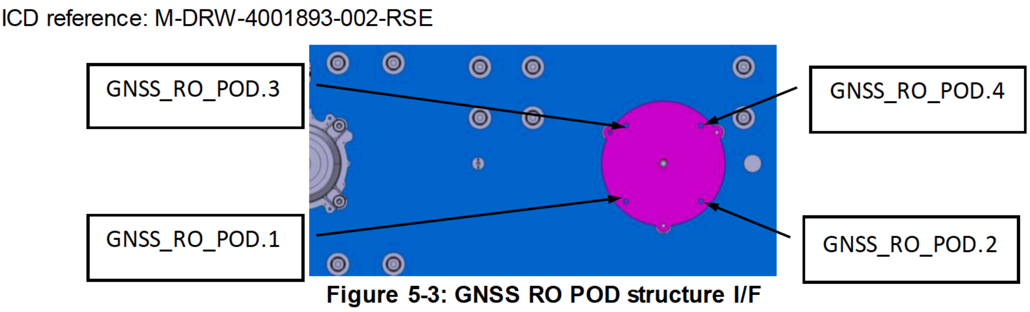

Figure 2-9 The position vector r_{RO-POD} is defined as the average of the four mounting holes of the antenna. These mounting points have been measured on the structure and are within positioning tolerances (0.1 mm) with a flatness measured at 0.001 mm

REQUIRED						OBTAINED				TOLERANCE				
GNSS-RO-POD ANTENNA						GNSS-RO-FORE ANTENNA				GNSS-RO-FORE ANTENNA				
AXIS REF. SPACE CRAFT (S/C)						AXIS REF. SPACE CRAFT (S/C)				AXIS REF. SPACE CRAFT (S/C)				
Points	REF.	$X_{S/C}$	$Y_{S/C}$	$Z_{S/C}$	TOL.	Points	$X_{S/C}$	$Y_{S/C}$	$Z_{S/C}$	Points	$X_{S/C}$	$Y_{S/C}$	$Z_{S/C}$	TOL
GNSS_RO_POD.1	$X_{S/C}$ $Y_{S/C}$ $Z_{S/C}$	557,5	42,5	-1095	only knowledge	GNSS_RO_POD.1	**557,503**	**42,057**	**-1095,096**	GNSS_RO_POD.1	0,003	-0,443	-0,096	**0,91**
GNSS_RO_POD.2	GNSS_RO_ POD.1	642,5	42,5	-1095	0.25 ref. GNSS_RO_ POD.1	GNSS_RO_POD.2	**642,503**	**42,119**	**-1095,016**	GNSS_RO_POD.2	0,000	0,062	0,080	0,20
GNSS_RO_POD.3		557,5	-42,5	-1095		GNSS_RO_POD.3	**557,401**	**-42,865**	**-1095,091**	GNSS_RO_POD.3	-0,102	0,078	0,005	0,26 1)
GNSS_RO_POD.4		642,5	-42,5	-1095		GNSS_RO_POD.4	**642,402**	**-42,942**	**-1095,018**	GNSS_RO_POD.4	-0,101	0,001	0,078	0,26 1)

Table 2-5 detailed metrology of GNSS-RO POD mounting interface point tolerances

Antenna patterns communicated above should be consulted to establish an estimate of phase centre.

2.4.5 *AMR-C reference frame origin in SRF, DCM and boresight vector*

The ideal radiometer reference frame is located at the centre of the AMR-C middle foot. The origin of this reference frame within the SRF is given by:

$$r_{AMR} = \begin{bmatrix} 3650.0 \\ 0.0 \\ -415.0 \end{bmatrix} \begin{bmatrix} X_s \\ Y_s \\ Z_s \end{bmatrix} \quad \text{mm}$$

[3] ftp://sentinel6-science:yot7+scart@ftp.eopp.esa.int/from_estec/POD-Context/Data/GNSS-RO-POD/

The DCM, rotating the SRF to the AMR-C reference frame is given by

$$A_{AMR} = \begin{bmatrix} 0.9982189812 & 0.0023453783 & -0.0596100896 \\ -0.0023191197 & 1.0000080916 & 0.0005107854 \\ 0.0596105371 & -0.0003678737 & 0.9982107135 \end{bmatrix}$$

The AMR-C boresight vector is given by the direction vector:

$$\vec{r}_{AMR-BS} = \begin{bmatrix} -0.0002621201 \\ 0.0004690117 \\ 0.999999857 \end{bmatrix} \begin{bmatrix} X_s \\ Y_s \\ Z_s \end{bmatrix}$$

2.4.6 GNSS-POD antenna phase centres and knowledge

Each satellite accommodates two GNSS-POD instruments. The first is the nominal instrument and antenna (GNSS-POD A) and the second is a redundant instrument that has also been used during satellite in-orbit verification for various signal tracking tests (GNSS-POD B).

2.4.6.1 GNSS POD antenna reference point

The position of the origins of the two GNSS-POD antenna reference frames within the satellite reference frame is given by

$$r_{GP1} = \begin{bmatrix} 2474.83 \\ 0.12 \\ -1080.31 \end{bmatrix} \begin{bmatrix} X_s \\ Y_s \\ Z_s \end{bmatrix} \quad \text{mm}$$

$$r_{GP2} = \begin{bmatrix} 2874.86 \\ 0.16 \\ -1080.54 \end{bmatrix} \begin{bmatrix} X_s \\ Y_s \\ Z_s \end{bmatrix} \quad \text{mm}$$

and are obtained by averaging 4 interface point measurements.

The *GNSS-POD A #1* antenna (model 34), r_{GP1}, is the nominal antenna to be used for the S6 MF GNSS-POD A instrument. The *GNSS-POD#2* antenna (model 35), r_{GP2}, is the redundant antenna for the S6 MF GNSS-POD B instrument.

The transformation from the spacecraft reference to the GNSS POD antenna reference frame is described by the following DCMs:

GNSS POD A antenna 1:

The DCM rotating the SRF to the GNSS-POD #1 reference frame is

$$A_{GP1} = \begin{bmatrix} 1.0 & -0.000707 & -0.000236 \\ -0.000707 & -1.0 & 0.0 \\ -0.000236 & 0.0 & -1.0 \end{bmatrix}$$

GNSS POD B antenna 2:

The DCM rotating the SRF to the GNSS-POD #2 reference frame is

$$A_{GP2} = \begin{bmatrix} -1.0 & 0.000470 & -0.000470 \\ 0.000470 & 0.999999 & -0.000118 \\ 0.000470 & -0.000118 & -0.999999 \end{bmatrix}$$

2.4.6.2 Phase centre and knowledge

The on-ground antenna stand-alone measured phase centres for the for the GNSS-POD antenna is provided here[4] the file Readme-POD-Docs-20201102.pdf.

The code and carrier range variations for L1, L2 and L5 are similar enough so that a common reference point can be used. The location of the ARP is defined in the Antenna Reference Frame (ARF).

2.4.7 DORIS antenna phase centre and knowledge

2.4.7.1 DORIS antenna reference point

The origin of the antenna reference frame is defined by the intersection between the RF axis (revolution axis which is the z-axis) of the antenna and the antenna mounting plate[5] and given by the following position vector for both 400 MHz and 2 GHz channels, with an accuracy of 1 mm.

$$r_{DOR} = \begin{bmatrix} 1625.061 \\ 399.288 \\ 685.242 \end{bmatrix} \begin{bmatrix} X_s \\ Y_s \\ Z_s \end{bmatrix} \quad \text{mm}$$

The transformation from the spacecraft reference to the DORIS antenna reference frame is given by the following matrix:

$$A_{DORIS} = \begin{bmatrix} 0.999999836 & 0.000357185 & -0.000447646 \\ 0.000356814 & -0.999999592 & -0.000829548 \\ -0.000447942 & 0.000829388 & -0.999999556 \end{bmatrix}$$

The resulting angle between the mechanical antenna axis and the nadir Z_s axis amounts to: 0.054°

2.4.7.2 DORIS antenna phase centre

The on-ground antenna stand-alone measured phase centres for both 400 MHz and 2 GHz channels are measured in the antenna reference frame.

The following table gives the position vector from the DORIS antenna reference point to the DORIS antenna centre of phase of the antenna

$$r_{DOR\_Ph\_DOR}^{401.25MHz} = \begin{bmatrix} 0.0 \\ 0.0 \\ 143.0 \end{bmatrix} \begin{bmatrix} X_s \\ Y_s \\ Z_s \end{bmatrix} \text{ mm with accuracy} \pm 5 \text{ mm}$$

$$r_{DOR\_Ph\_DOR}^{2036.25MHz} = \begin{bmatrix} 0 \\ 0 \\ 312.0 \end{bmatrix} \begin{bmatrix} X_s \\ Y_s \\ Z_s \end{bmatrix} \text{ mm with accuracy} \pm 5 \text{ mm}$$

2.4.7.3 DORIS antenna phase laws

The azimuth and elevation antenna phase laws for the Sentinel-6A DORIS MV26 antenna are:

Accuracy of the phase variation law in azimuth for 400 MHz and 2 GHz is:

- $Acc(Az_{400MHz})$: ±3.6°
- $Acc(Az_{2GHz})$: ±4.8°

Accuracy of the phase variation law in elevation for 400 MHz and 2 GHz is:

---

4 ftp://sentinel6-science:yot7+scart@ftp.eopp.esa.int/from_estec/POD-Context/Data/GNSS-POD-Context

5 Hence, the instrument Z_a axis if perfectly aligned would be equal to $-Z_S$.

- Acc(El_{400MHz}): ±2°
- Acc(El_{2GHz}): ±2.8°

The phase variation law in azimuth is close to a linear function of Azimuth
Phase(Az) = Az

The phase variation law in elevation can be considered a constant
Phase(El) = 0

2.5 Star tracker reference information

The star tracker axes are defined with x and y following the edges of the mounted electronic box and z axis following the boresight.

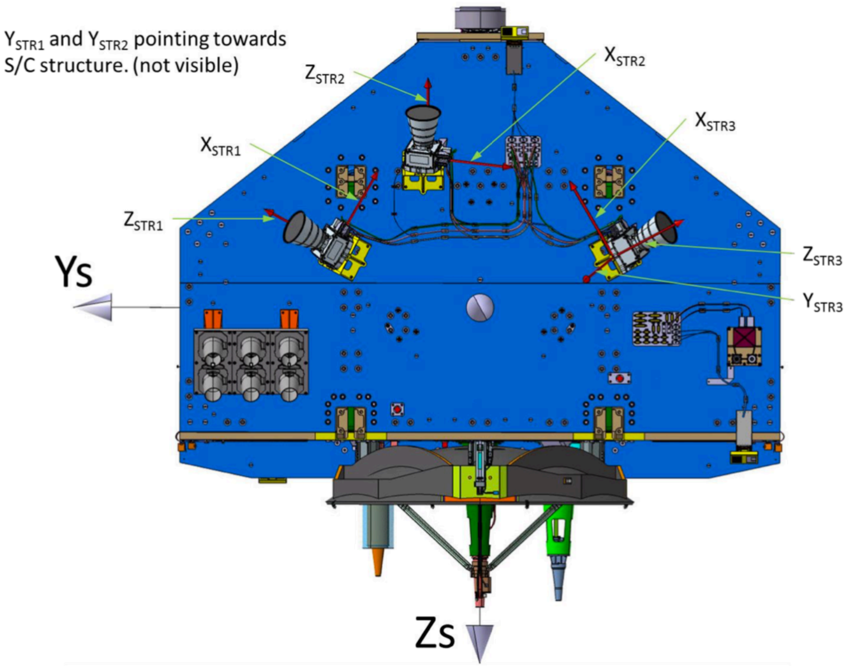

Figure 2-10 Location of the three star tracker camera heads and baffles.

The origin of the star tracker reference is centred at the bottom of the mounting with z-axis directed through the camera boresight. The position vectors or the origins in the SRF are:

$$r_{STR1} = \begin{bmatrix} 3674.428 \\ 574.471 \\ -240.02 \end{bmatrix} \begin{bmatrix} X_s \\ Y_s \\ Z_s \end{bmatrix} \quad \text{mm}$$

$$r_{STR2} = \begin{bmatrix} 3678.360 \\ 260.642 \\ -590.064 \end{bmatrix} \begin{bmatrix} X_s \\ Y_s \\ Z_s \end{bmatrix} \quad \text{mm}$$

$$r_{STR3} = \begin{bmatrix} 3803.572 \\ 525.529 \\ -199.980 \end{bmatrix} \begin{bmatrix} X_s \\ Y_s \\ Z_s \end{bmatrix} \quad \text{mm}$$

The transformation from the spacecraft reference frame into the star tracker reference frames are described by the following DCMs:

$$A_{STR1} = \begin{bmatrix} 0.07716410 & -0.50225910 & -0.86126749 \\ -0.89189474 & 0.35131488 & -0.28478257 \\ 0.44569498 & 0.79010164 & -0.42082729 \end{bmatrix}$$

$$A_{STR2} = \begin{bmatrix} 0.23067529 & -0.96600587 & 0.11670772 \\ -0.86826493 & 0.25854368 & -0.42340537 \\ 0.43918627 & -0.00366367 & -0.89838811 \end{bmatrix}$$

$$A_{STR3} = \begin{bmatrix} 0.08472368 & 0.50183916 & -0.86080158 \\ 0.89727937 & 0.33721868 & 0.28490927 \\ 0.43327299 & -0.79651205 & -0.42171445 \end{bmatrix}$$

The post-launch star tracker reference frames were updated on-board 2021-01-18 09:12 and are provided below.

$$A'_{STR1} = \begin{bmatrix} 0.07749282 & -0.50188388 & -0.86145657 \\ -0.89179974 & 0.35141553 & -0.28495675 \\ 0.44574442 & 0.79032885 & -0.42034774 \end{bmatrix}$$

$$A'_{STR2} = \begin{bmatrix} 0.23064078 & -0.96605013 & 0.11641295 \\ -0.86819331 & -0.25833296 & -0.42367966 \\ 0.43936909 & -0.00335114 & -0.89830038 \end{bmatrix}$$

$$A'_{STR3} = \begin{bmatrix} 0.08426275 & 0.49926641 & -0.86234149 \\ 0.89779653 & 0.33739383 & 0.28306676 \\ 0.43227442 & -0.79805918 & -0.41980992 \end{bmatrix}$$

2.5.1 *Post-Launch Star Tracker Alignment Exercise*

Between 3rd and 4th Aug 2021 an experiment was conducted to collect data from all three unblinded star trackers to assess relative pointing statistics. There was no eclipse and thus reduced thermoelastic variations.
Using star tracker #3 as the reference the following plots are found.

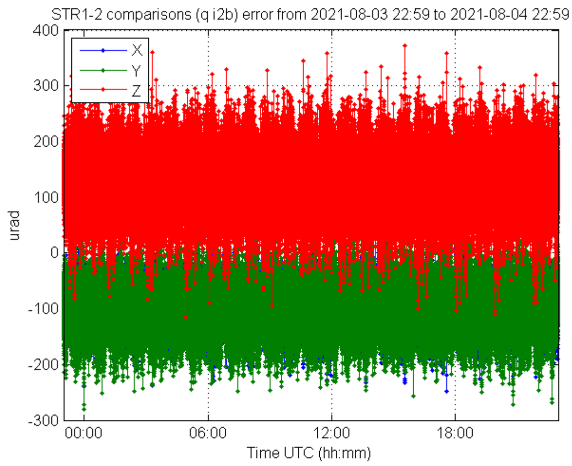

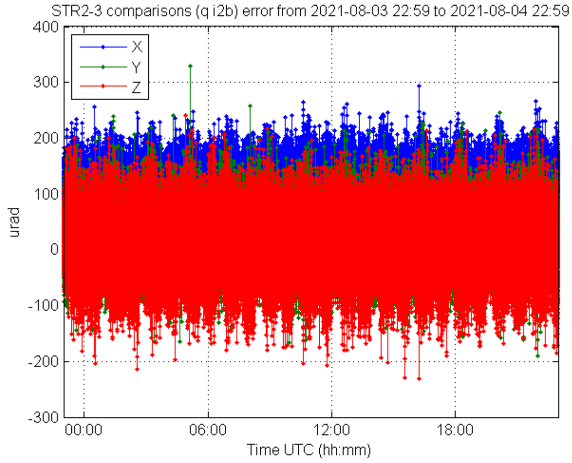

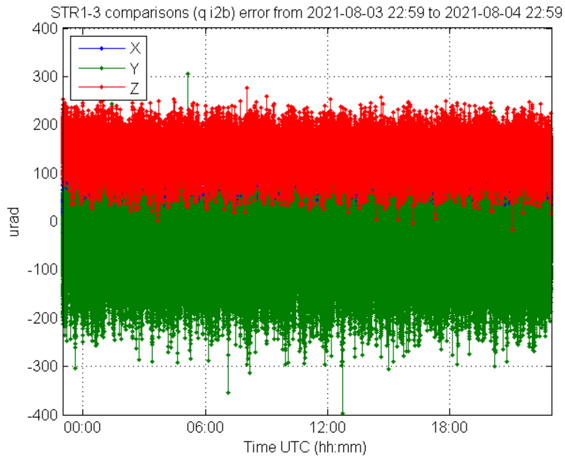

Figure 2-11 Angular offset in body frame between all STRs in eclipse-free Normal Mode Attitude Hold. The assessment shown is during daylight only using the on-board body-alignment quaternions pertaining to the day-night average.

The statistics relating to these alignments are provided in the following Table 2-6

Aug 3-4									
	STR 1 vs 3	micro rad	X	Y	Z	Milli Deg	X	Y	Z
		Mean	197.00	-67.60	134.90		11.29	-3.87	7.73
		SD	32.50	54.90	29.00		1.86	3.15	1.66
		Max abs	175.60	306.10	276.10		10.06	17.54	15.82
	STR 1 vs 2	micro rad	X	Y	Z	Milli Deg	X	Y	Z
		Mean	115.00	28.00	9.30		6.59	1.60	0.53
		SD	30.40	54.90	29.00		1.74	3.15	1.66
		Max abs	293.10	329.40	240.70		16.79	18.87	13.79

Table 2-6 Statistics of inter alignment of star trackers relative to star tracker #3

The mean misalignments on some axes are slightly larger than that assumed in the AOCS analysis and pointing requirement verification budget (57µrad or 3.266mDeg per axis) but the order of magnitude is comparable for all three star trackers. Note that the mean errors are established by taking an average over day and night segments. The assessment shown in Figure 2-11 is provided only during daylight using the on-board body-alignment quaternions pertaining to the day-night average.

Based on these data it was deemed unnecessary to tune the AOCS, though this position might change in the future in which case this document will be updated.

2.6 Laser Retroreflector Array reference information

The LRA onboard Sentinel-6 is manufactured by ITE Inc. and is the same model of the units flown on the Jason-2 and Jason-3 missions. The unit has 9 cubes on a spherical surface, as shown in Figure 2-12. The cubes are manufactured from SUPRASIL-1 (quartz) and have a diameter of approximately 32 mm. They have a refractive index of 1.46071 for a wavelength of 0.532 microns, and a group refractive index of 1.4853 for a wavelength of 0.532 microns. Nominally, no obscuration of the cubes can occur, but they can be obscured by MLI at very high off-nadir angle measurements. The back-face coating material is MgFI2.

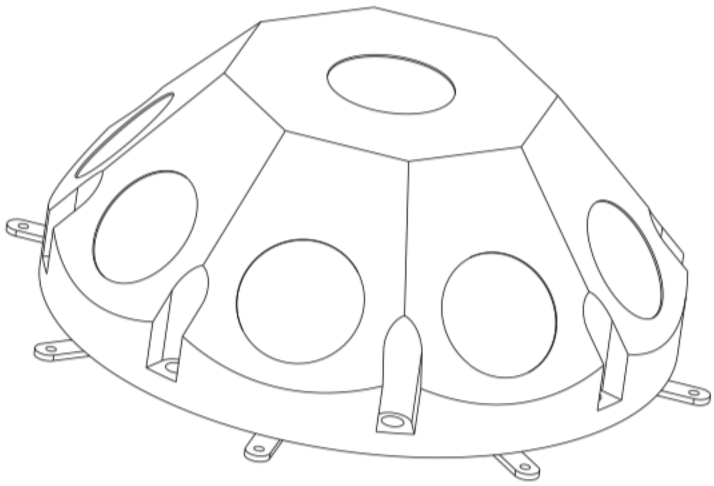

Figure 2-12 Sentinel-6 LRA

The position of the origin of the LRA reference frame in the spacecraft reference frame defined by, $r_{LRA-ICD}$, both from the Mechanical Interface Control Document and as measured. The origin of the LRA reference frame is located at the baseplate of the LRA, with the X and Y axes lying in the plane of the baseplate. The Z-axis of the LRA reference frame effectively points outward to the top-facing cube. The reference frame origin, r_{LRA}, accounts for the thickness of the LRA bracket and the LRA washers. The orientation of the LRA in the spacecraft reference frame is given by the DCM $A_{LRA-ICD}$ and the optical centre of the LRA in the LRA reference frame is given by $r_{LRA-LRA}$and illustrated in Figure 2-13. The location and orientation of the individual cubes in the LRA are provides in Table 2-7.

Hence, the ICD defined position vector for the LRA reference frame origin within the SRF is given by

$$r_{LRA-ICD} = \begin{bmatrix} 1625.0 \\ -400.0 \\ 688.175 \end{bmatrix} \begin{bmatrix} X_s \\ Y_s \\ Z_s \end{bmatrix} \quad \text{mm}$$

And the measured value is

$$r_{LRA} = \begin{bmatrix} 1624.813 \\ -400.605 \\ 688.152 \end{bmatrix} \begin{bmatrix} X_s \\ Y_s \\ Z_s \end{bmatrix} \qquad \text{mm}$$

The transformation from the spacecraft reference frame into the LRA reference frame are described by the following DCMs concerning the ICD and those measured :

$$A_{LRA-ICD} = \begin{bmatrix} -0.707107 & -0.707107 & 0.0 \\ 0.707107 & -0.707107 & 0.0 \\ 0.0 & 0.0 & 1.0 \end{bmatrix}$$

$$A_{LRA} = \begin{bmatrix} -0.7069449749 & -0.7072661170 & 0.0018553350 \\ 0.7072675079 & -0.7069460046 & 0.0001374387 \\ 0.0012144160 & 0.0014093798 & 0.9999982694 \end{bmatrix}$$

The position of the LRA optical centre in the LRA reference frame are given by

$$r_{LRA-LRA} = \begin{bmatrix} 0.0 \\ 0.0 \\ -23.375 \end{bmatrix} \begin{bmatrix} X_{LRA} \\ Y_{LRA} \\ Z_{LRA} \end{bmatrix} \qquad \text{mm}$$

Note that a range correction to the measured range is required to move the point of optical reflection to the optical center of the LRA. The optical centre defined in Figure 2 is the centre of a sphere on which the front faces of the retroreflector cubes are tangent. Range corrections are also shown in the figure, representing the error window for a given line of sight or incidence angle (θ,φ) on the array. Adding the range correction to the measured range adjusts the apparent point of reflection to the optical centre of the retroreflector array. Alternatively, and if desired, the incidence angle dependence could be removed by using instead an average range correction of 4.6 cm across the entire array

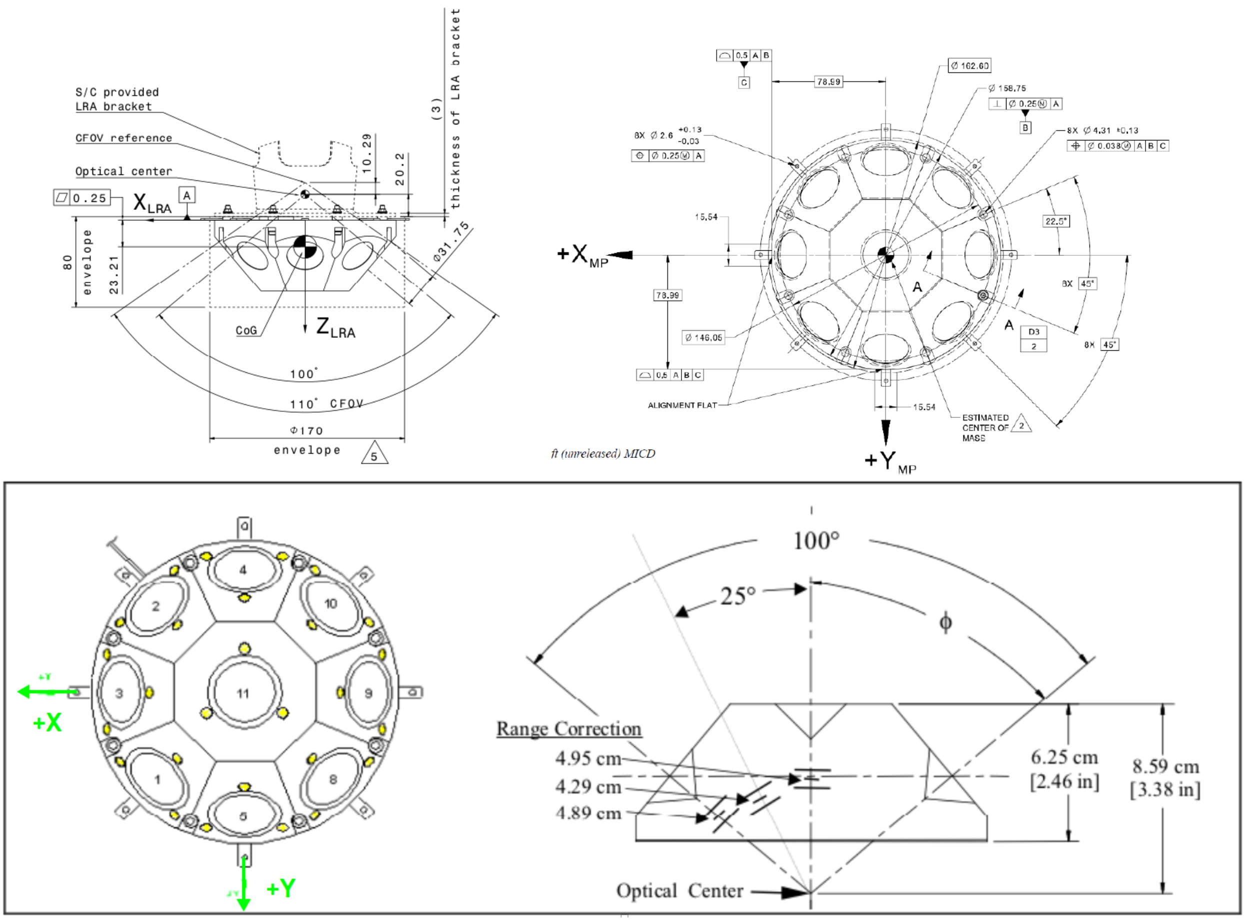

Figure 2-13 LRA field of view (FOV) and coordinate system. The Z-axis of the LRA reference frame points toward nadir.

Cube SN	X	Y	Z	θ	θ
3	0.06324	0.00000	0.05306	0.00000	0.87266
1	0.04472	0.04472	0.05306	0.78540	0.87266
5	0.00000	0.06324	0.05306	1.57080	0.87266
8	-0.04472	0.04472	0.05306	2.35619	0.87266
9	-0.06324	0.00000	0.05306	3.14159	0.87266
10	-0.04472	-0.04472	0.05306	3.92699	0.87266
4	0.00000	0.06324	0.05306	4.71239	0.87266
2	0.04472	-0.04472	0.05306	5.49779	0.87266
11	0.00000	0.00000	0.00000	0.00000	0.00000

Table 2-7 Retroreflector Array Coordinates. Units are m and radians.

Satellite laser ranging measurements from the Sentinel-6 mission are used to support precise orbit determination of the satellite, and/or validation of precise orbit determination performed using other tracking systems (e.g., GNSS, DORIS). The International Laser Ranging Service (https://ilrs.cddis.eosdis.nasa.gov), a service of the International Association of Geodesy, coordinates activities for the international network of laser ranging field stations, with the network representing a global consortium of permanent and mobile field stations. The ILRS collects and distributes laser ranging measurements from the network to the passive Laser Retroreflector Array (LRA) on Sentinel-6.

3 Orbit Parameters

3.1 Reference orbit

The Sentinel-6 nominal orbit is derived from historical analysis of the Jason-2 orbit data from 2008 to 2016 given in the next table in True-of-Date mean Keplerian elements. The Sentinel-6 satellites will have the same ground track as Jason-2 and Jason-3 with a 30 second in an extended ~16 month tandem phase. The assumed Earth gravity constant, μ, is 3.98600442 10^{14} m^3s^{-2}.

Description	Symbol	Value
semi-major axis [km]	a	7714.432
Eccentricity [-]	e	0.000098
Inclination [deg]	i	66.042

Table 3.1 Sentinel-6 True-of-Date Mean Orbital Elements

The orbit parameters above result in the following:

Description	Symbol	Value
Nodal period (s)		6745.7605
Orbits per day (orbits/day)		12.808
Repeat cycle (days)		9.91564
Orbits per cycle		127
RAAN rate (Degrees/day)		-2.07707
Mean separation between tracks at the equator (km)		315.55
Acute angle at equator crossings (Degrees)		39.4
Orbital velocity (km/s)		7.2
Ground track velocity (km/s)		5.8

3.2 Payload Calibration Manoeuvres

3.2.1 AMR-C pitch manoeuvre

In order to perform the radiometer calibration, it is required to execute an attitude manoeuvre to achieve cold sky pointing. This attitude manoeuvre sequence consists of the following steps:

1. Transition #1 from Nominal Attitude Frame to Nominal Frame rotated ≥+80° around the satellite Y_S axis. Transition period ~400 s.
2. Calibration - the radiometer calibration constraints are
   i. Satellite over land to minimise loss of Poseidon-4 data.
   ii. Duration several seconds
3. Transition #2 from Nominal Attitude Frame rotated ≥+80° around the satellite Y_S axis to Nominal Frame. Transition period ~400 s.

3.2.2 Poseidon-4 calibration manoeuvres

Regarding the altimeter attitude calibration during commissioning, several combinations of small manoeuvres alternatively on pitch and roll axis (+/- 0.4°) have been performed.

Step	Roll (X_S) [deg off nadir]	Pitch (Y_S) [deg off-nadir]	Duration [min]	Note
1	+0.4	0	20	The 20 minutes covers the transferring from nominal pointing to the bias and back to nominal pointing.
2	-0.4	0	20	
3	0	+ 0.4	20	
4	0	- 0.4	20	
5	-0.4	-0.4	20	
6	+0.4	+0.4	20	

In addition, tests have been carried out with an applied yaw bias of ±90° in order to allow assessment of the Poseidon-4 electrical boresight pointing in the spacecraft Y-axis. These tests are ideally carried out with 20 minutes of SAR recording with no roll or pitch bias.

3.2.3 180°yaw bias manoeuvres to support POD

In order to support POD activities during commissioning the platform was, on three occasions, yaw biased by 180° for ~4 days around the solar beta angle of ~0°. The following table provides the start and stop times of the manoeuvres as of the date of this document. Future manoeuvres are TBD.

Manoeuvre	Start: Slew start/stop (UTC)	End: Slew start – stop (UTC)	Comment
1	01/07/2021 13:08z – 13:12z	05/07/2021 12:56z - 13:00z	
2	01/09/2021	05/09/2021	See NAVATT manoeuver flags
3	05/11/2021 16:26z	09/11/2021 17:29z	
4	27/02/2022 16:03:24z	03/03/2022 17:12:21z	Period within 180° bias
5	25/04/2022 16:53z	29/04/2022 16:36z	Period within 180° bias

Table 3-1 Dates of 180° yaw flips

3.2.4 90° yaw bias manoeuvres in support of altimeter boresight pointing

In order to support determination of altimeter boresight misalignment studies in the satellite Y_S axis a ±90° yaw bias was applied at the following times.

Manoeuvre	Start	End:	Comment
1	Slew start from 0°: 19/11/2021 03:52:45 Altimeter experiment start: 19/11/2021 04:14:21.632	Altimeter experiment end: 19/11/2021 04:27:45 Slew start from+90° 19/11/2021 04:38:25	+90° yaw bias applied.
2	Slew start from 0°: 19/11/2021 16:13:21.000 Altimeter experiment start: 19/11/2021 16:35:02.776	Altimeter experiment end: 19/11/2021 16:48:25 Slew start from+90° 19/11/2021 16:59:00.000	-90° yaw bias applied
3	Slew start from 0°: 17/01/2022 15:42:57 Altimeter experiment start: 17/01/2022 16:05:30	Altimeter experiment end: 17/01/2022 16:12:20 Slew start from+90° 17/01/2022 16:18:55	+90° yaw bias applied.
4	Slew start from 0°: 18/01/2022 04:03:34 Altimeter experiment start: 18/01/2022 04:26:11	Altimeter experiment end: 18/01/2022 04:32:54 Slew start from-90° 18/01/2022 04:39:32	-90° yaw bias applied

Table 3-2 Dates of ±90° yaw bias manoeuvres

4 SATELLITE CONFIGURATION AND PHOTOGRAPHS

The following drawing shows the spacecraft with DSP in the deployed configuration. The full resolution image is attached to the PDF.

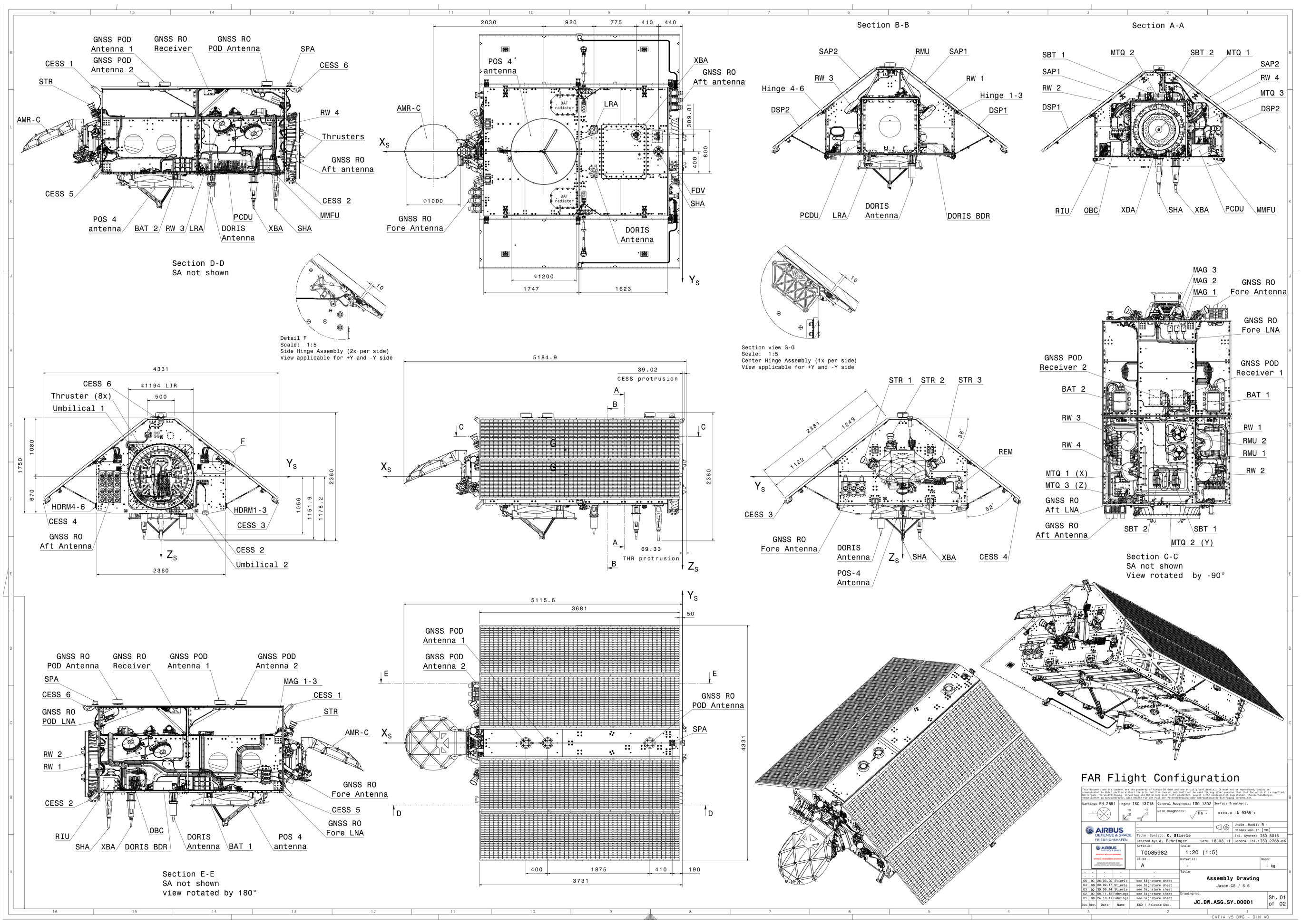

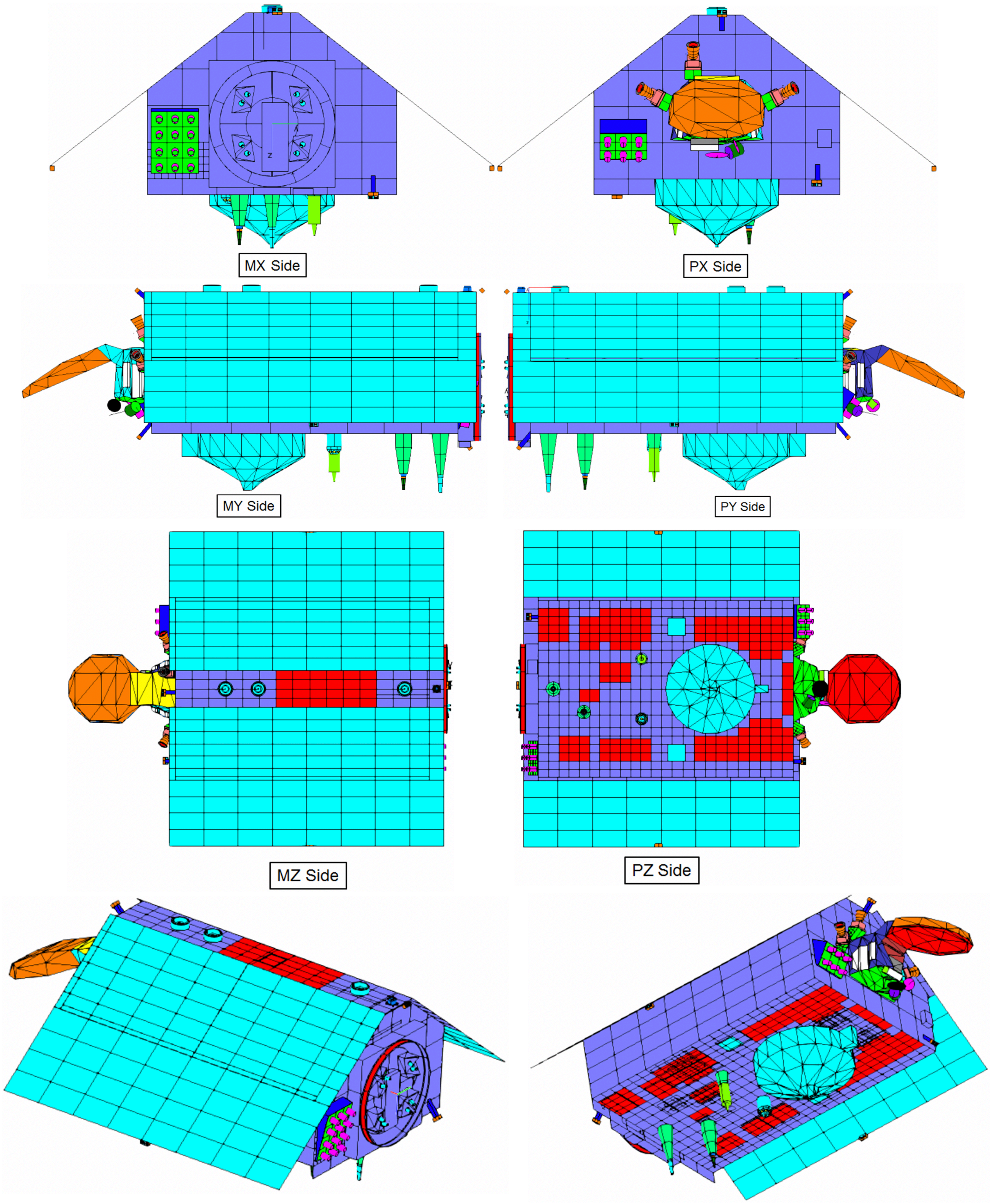

Figure 4-1 Different orientations of the spacecraft with 'P' meaning the projection from the positive X, Y or Z axis and 'M' from the negative X, Y or Z axis.

4.1 Spacecraft surface photographs

Photographs of all external surfaces and MLI overlaps have been taken prior to the shipment of the Sentinel-6 MF satellite to the launch facility for final post shipment testing.

.

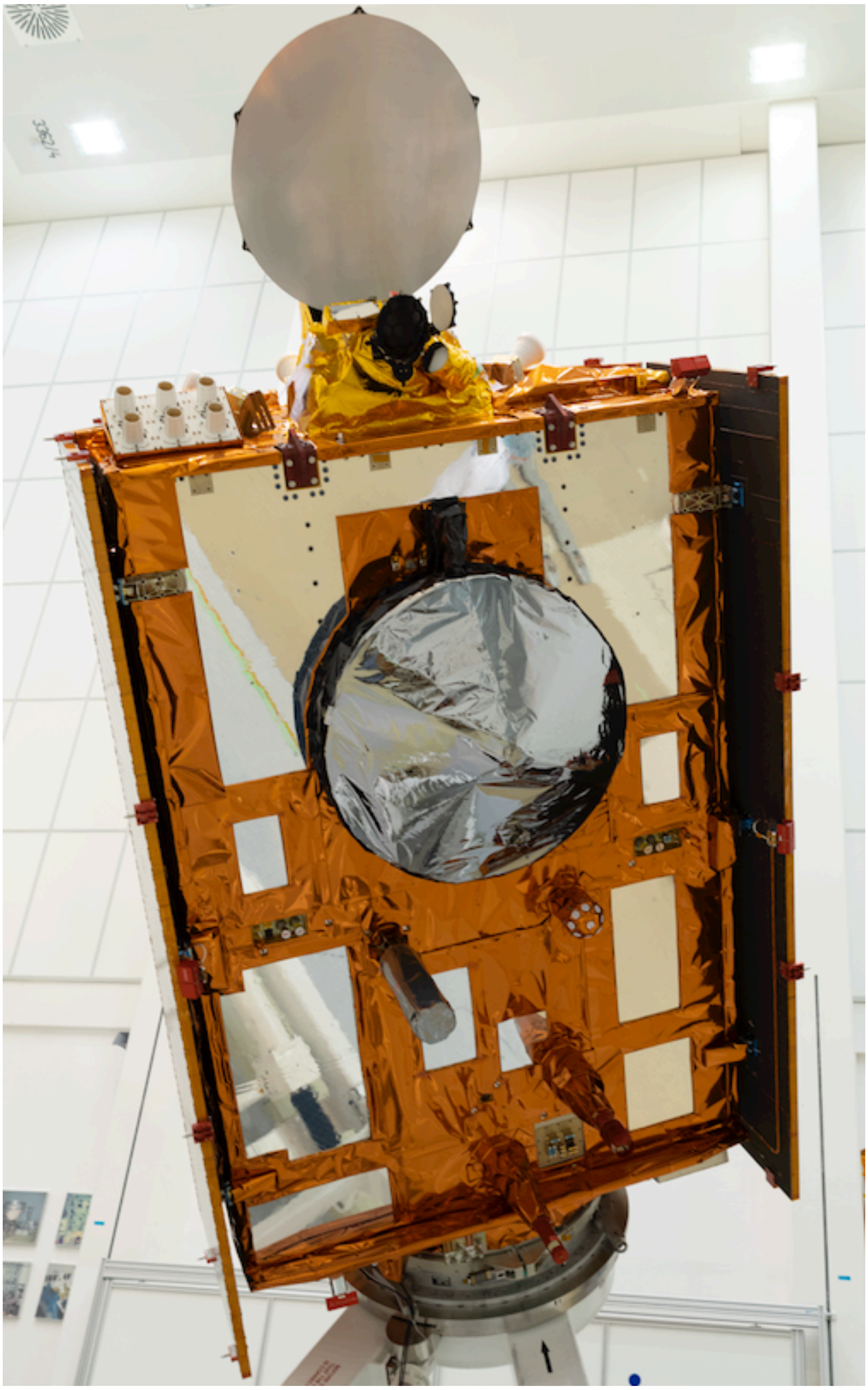

Figure 4-2

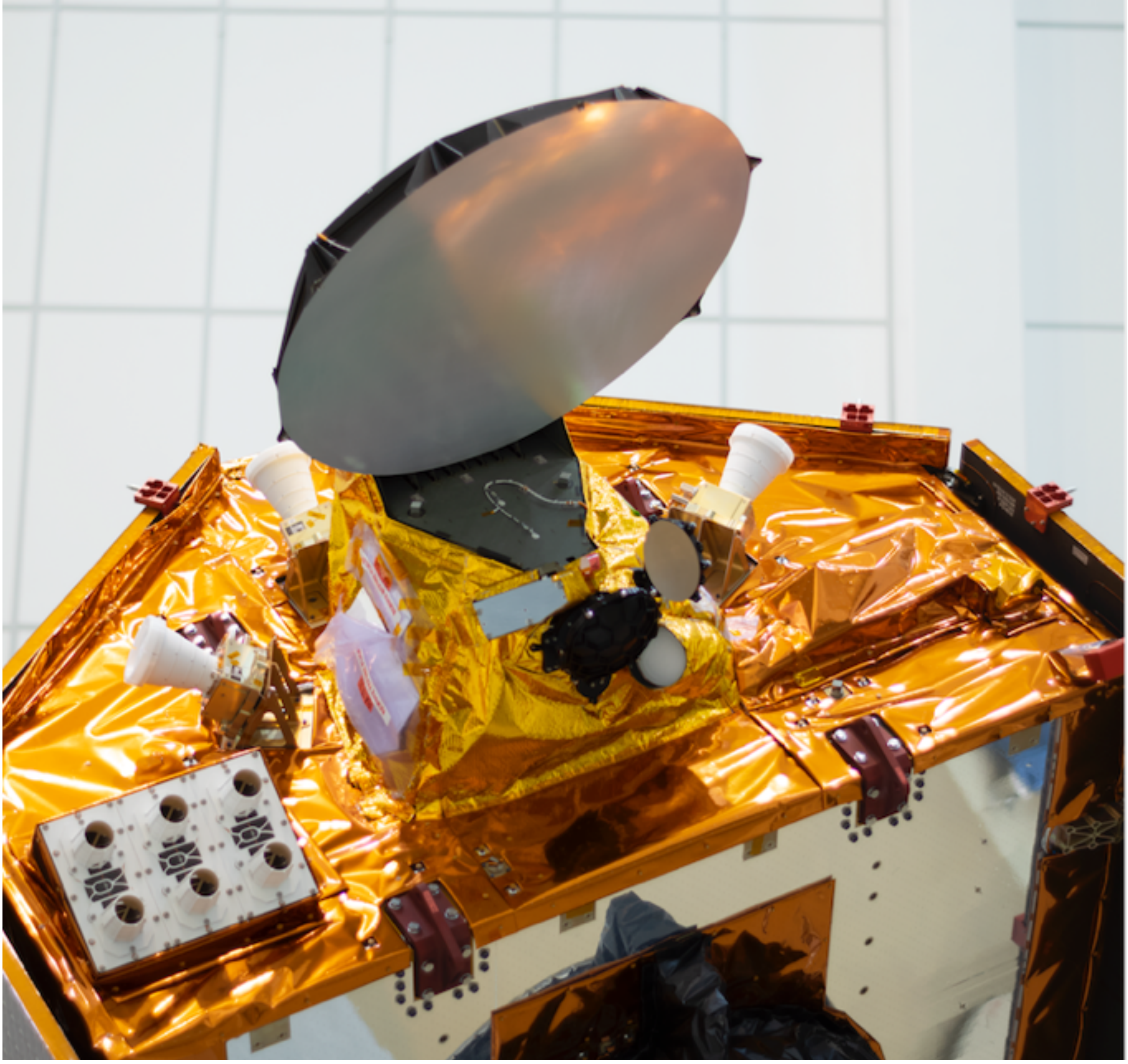

Figure 4-3

Figure 4-4

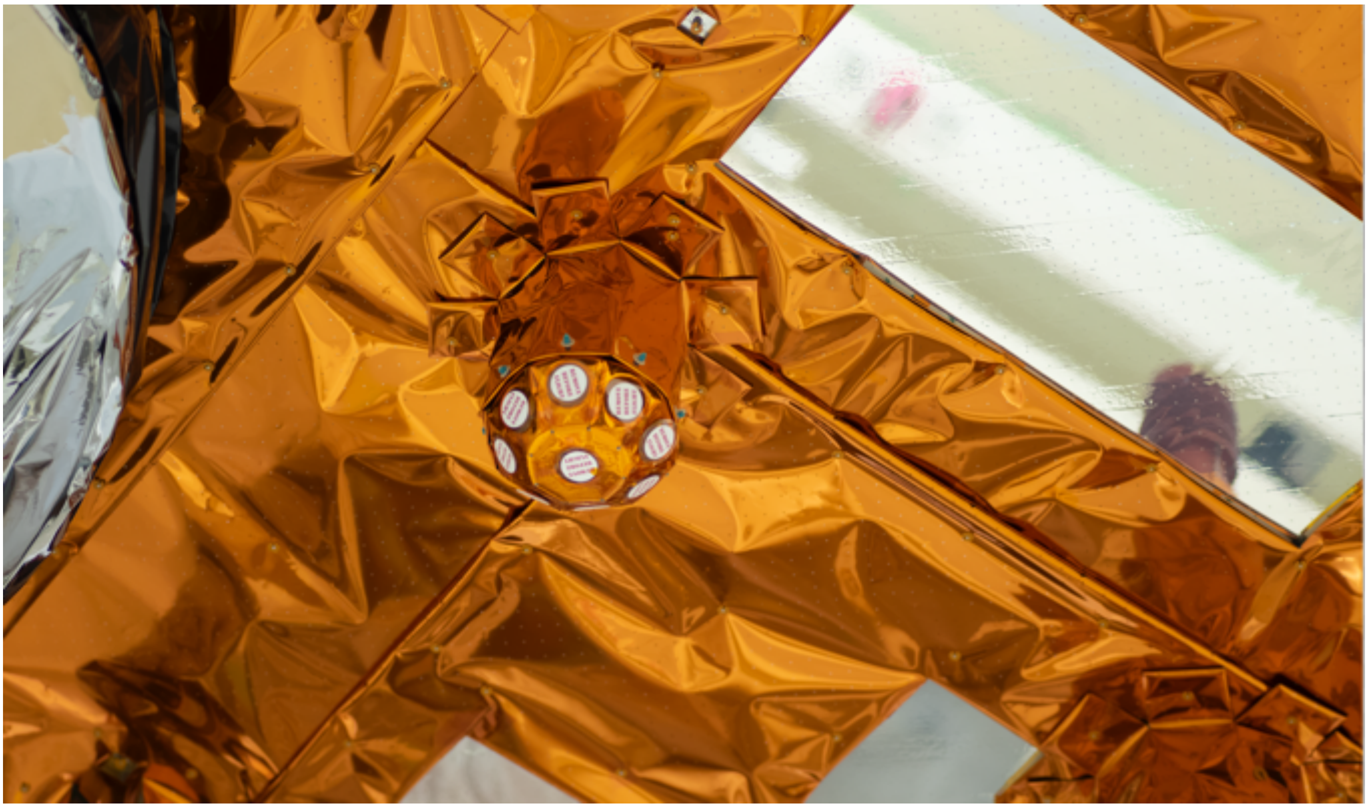

Figure 4-5

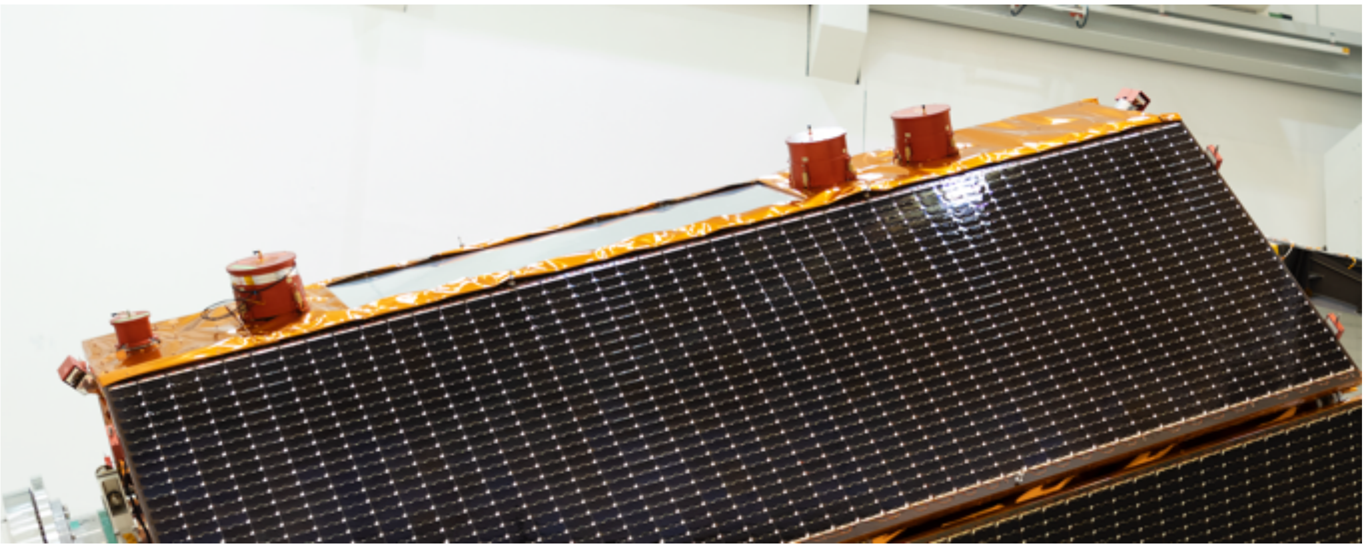

Figure 4-6

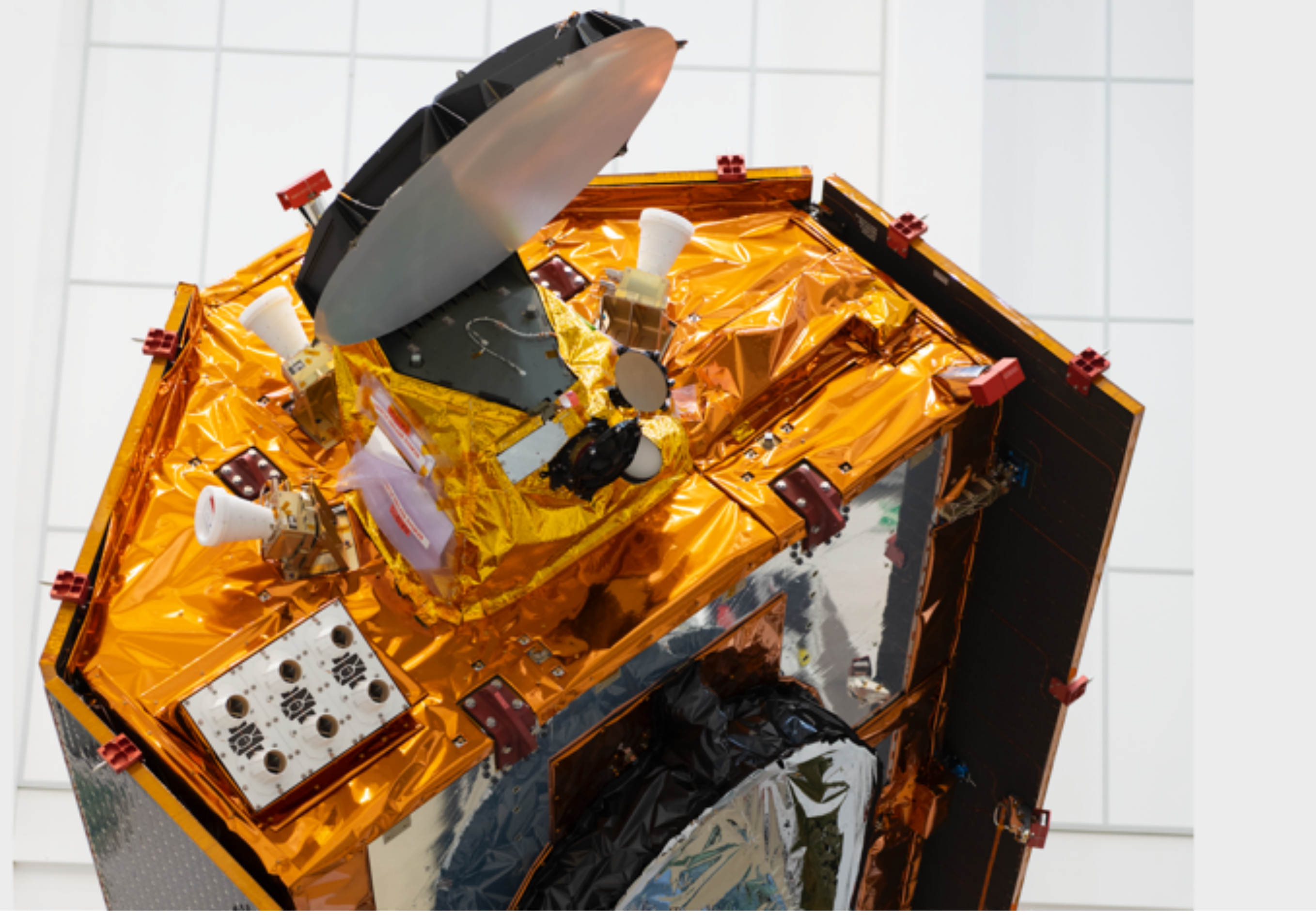

Figure 4-7

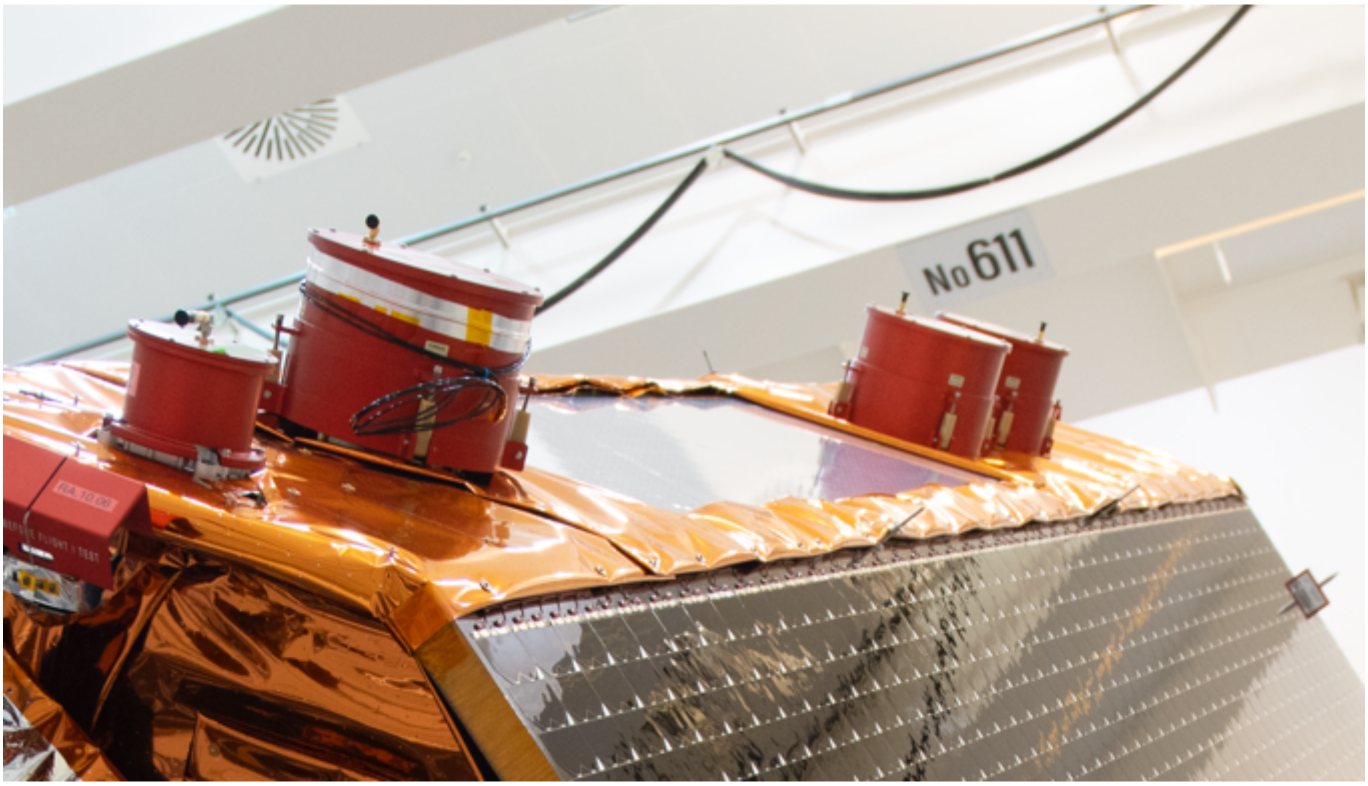

Figure 4-8

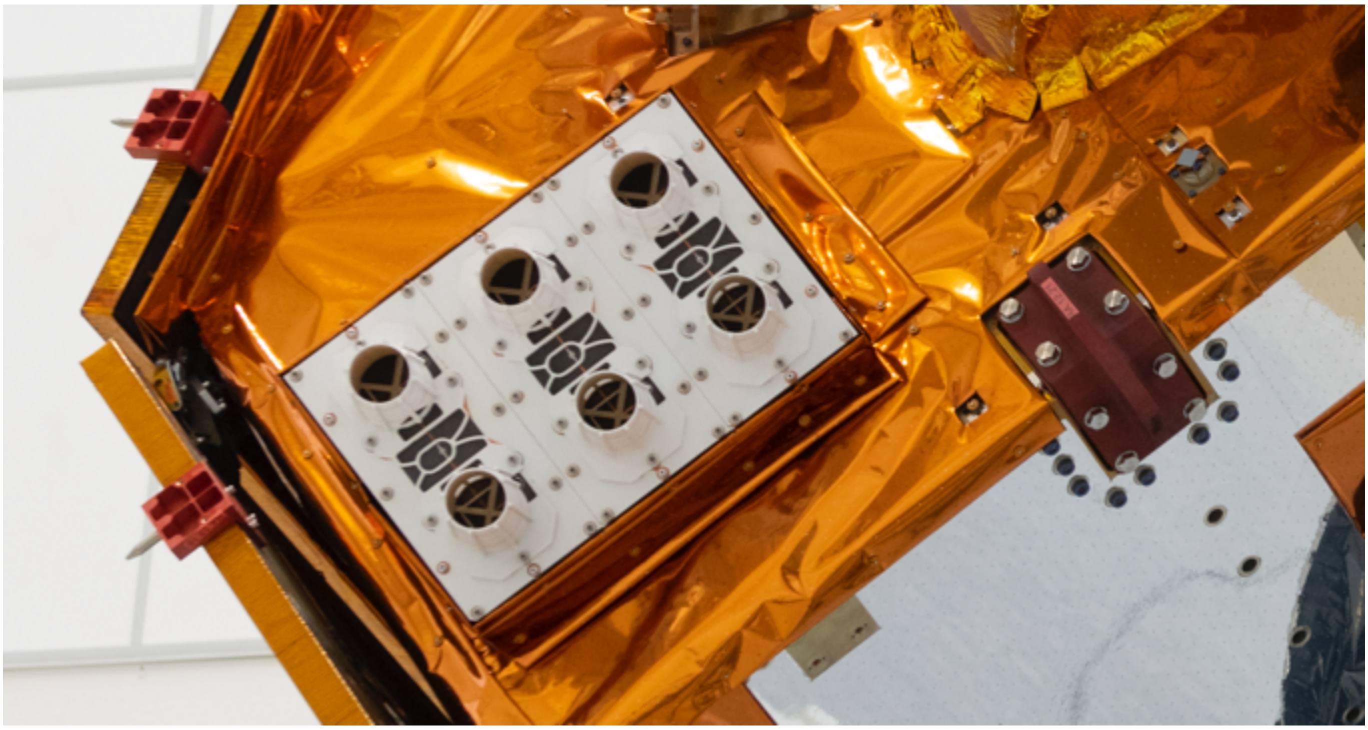

Figure 4-9

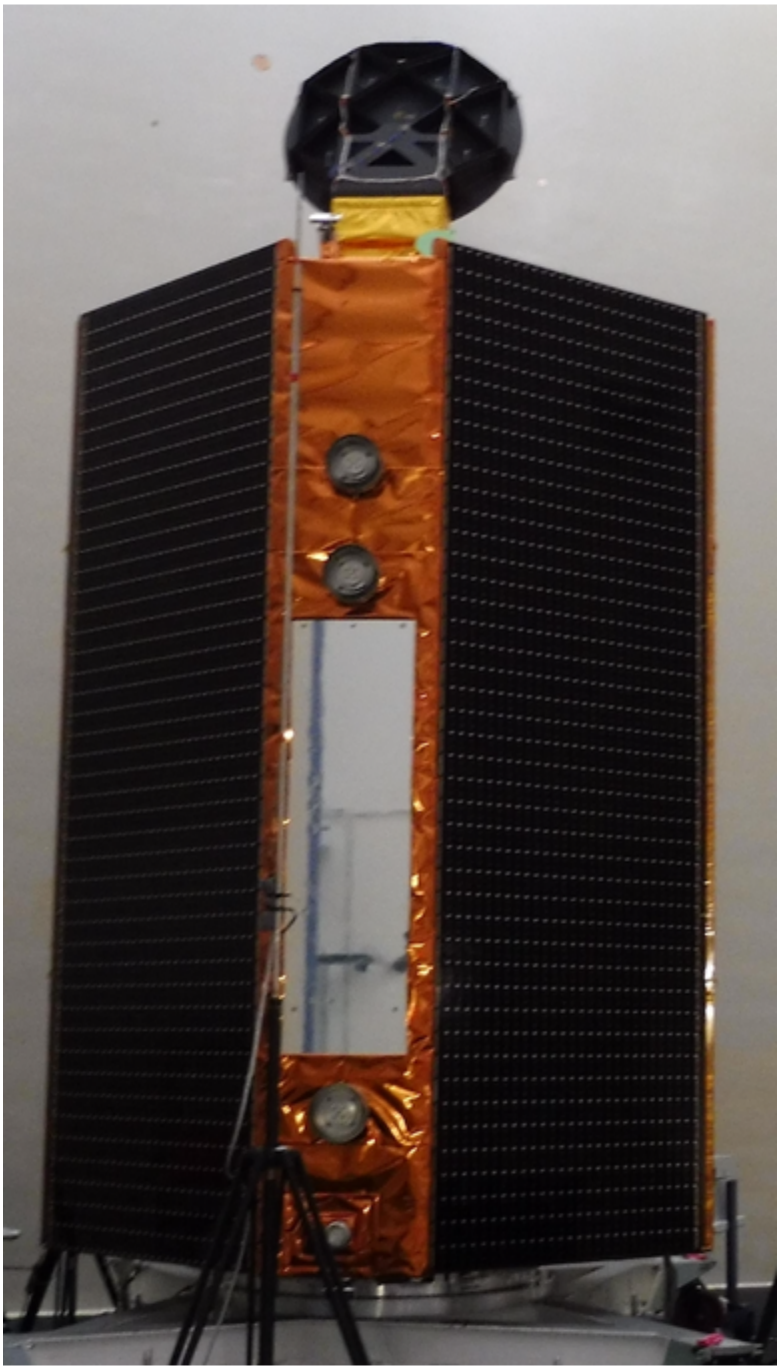

Figure 4-10

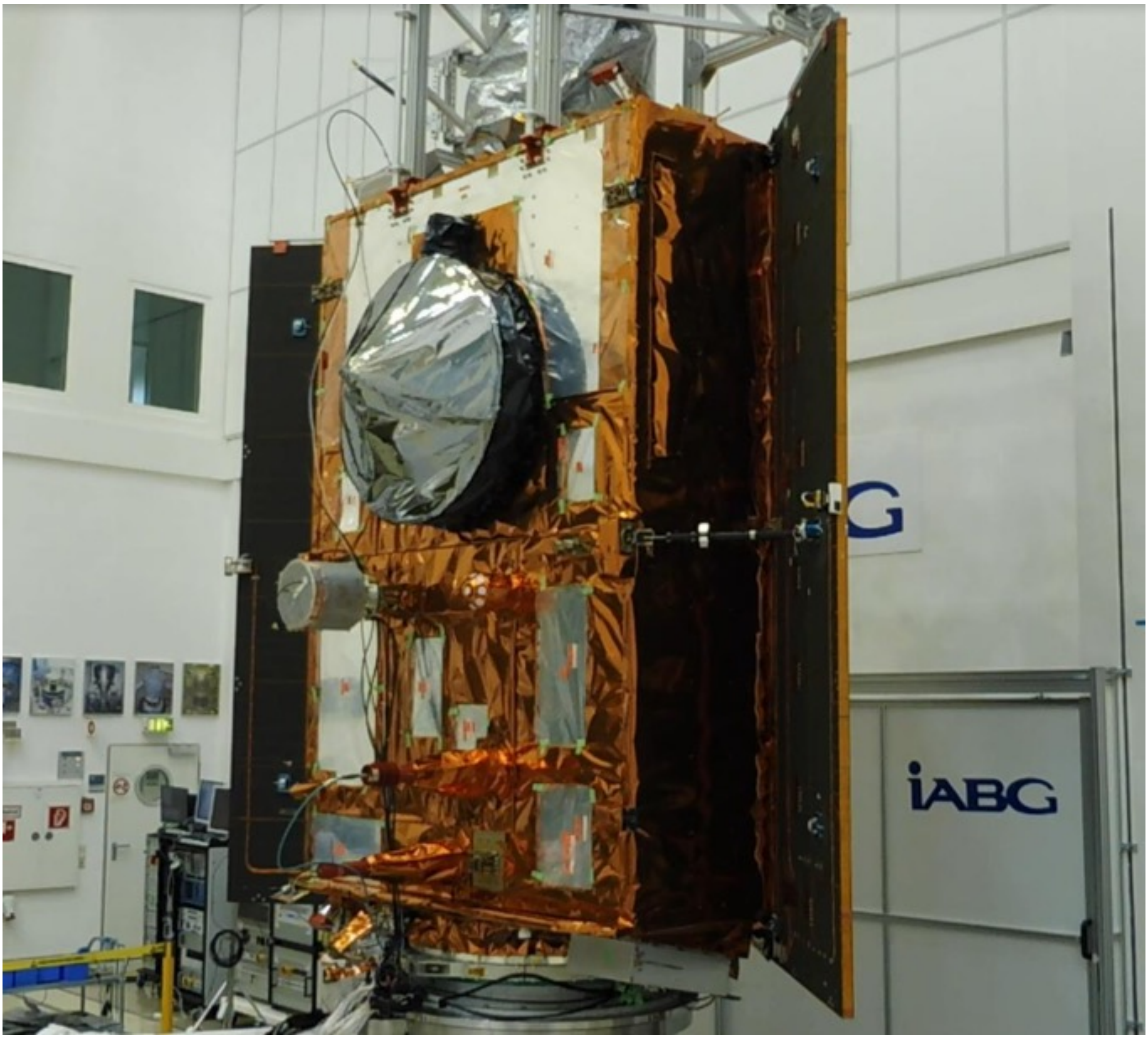

Figure 4-11

4.2 Photographs prior to spacecraft fuelling

Photographs of all external surfaces and MLI overlaps have been taken prior to the satellite encapsulation within the Falcon-9 fairing. A selection is provided below.

Figure 4-12 GNSS-RO POD antenna (right)

Figure 4-13 GNSS-POD nominal antenna

Figure 4-14 GNSS-POD redundant antenna

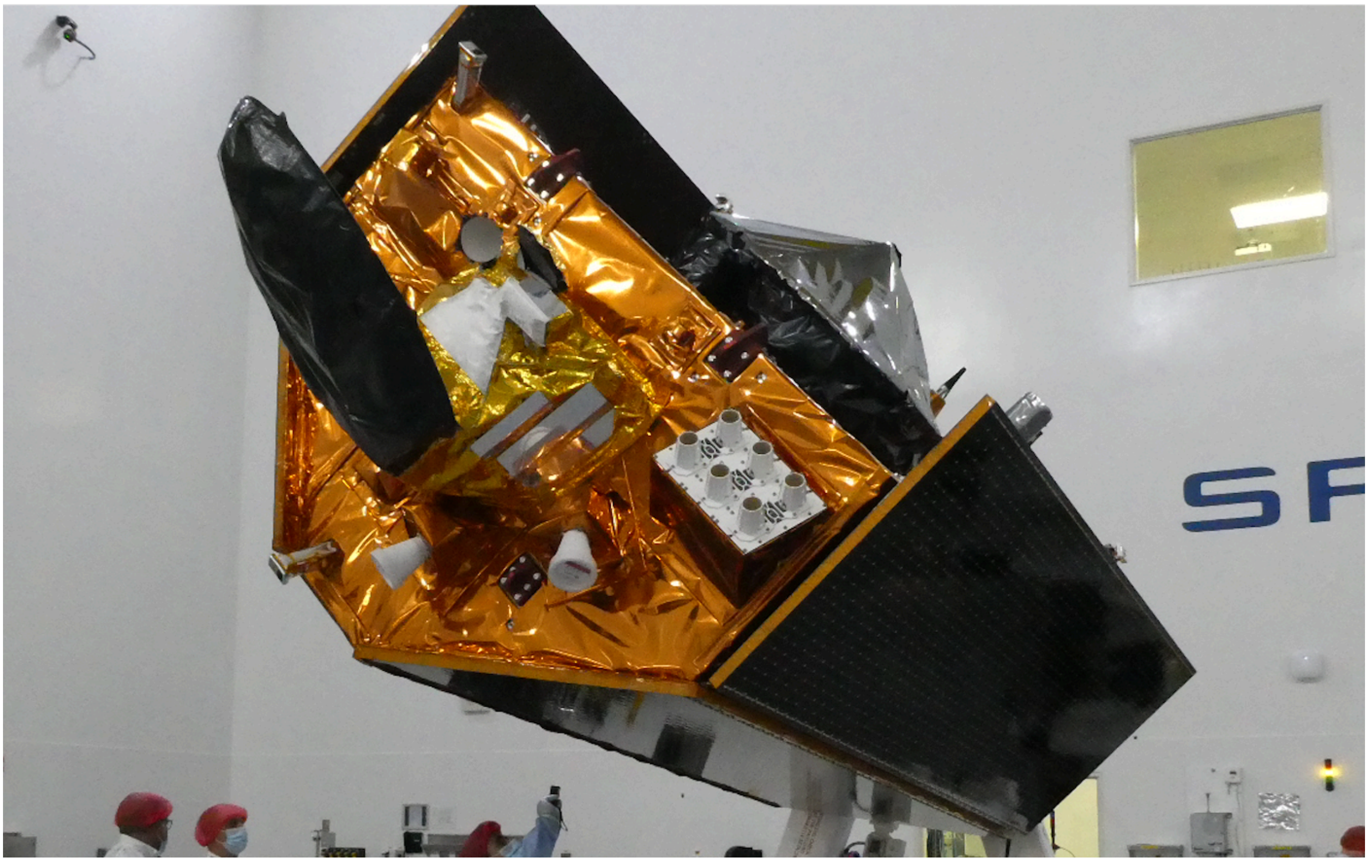

Figure 4-15

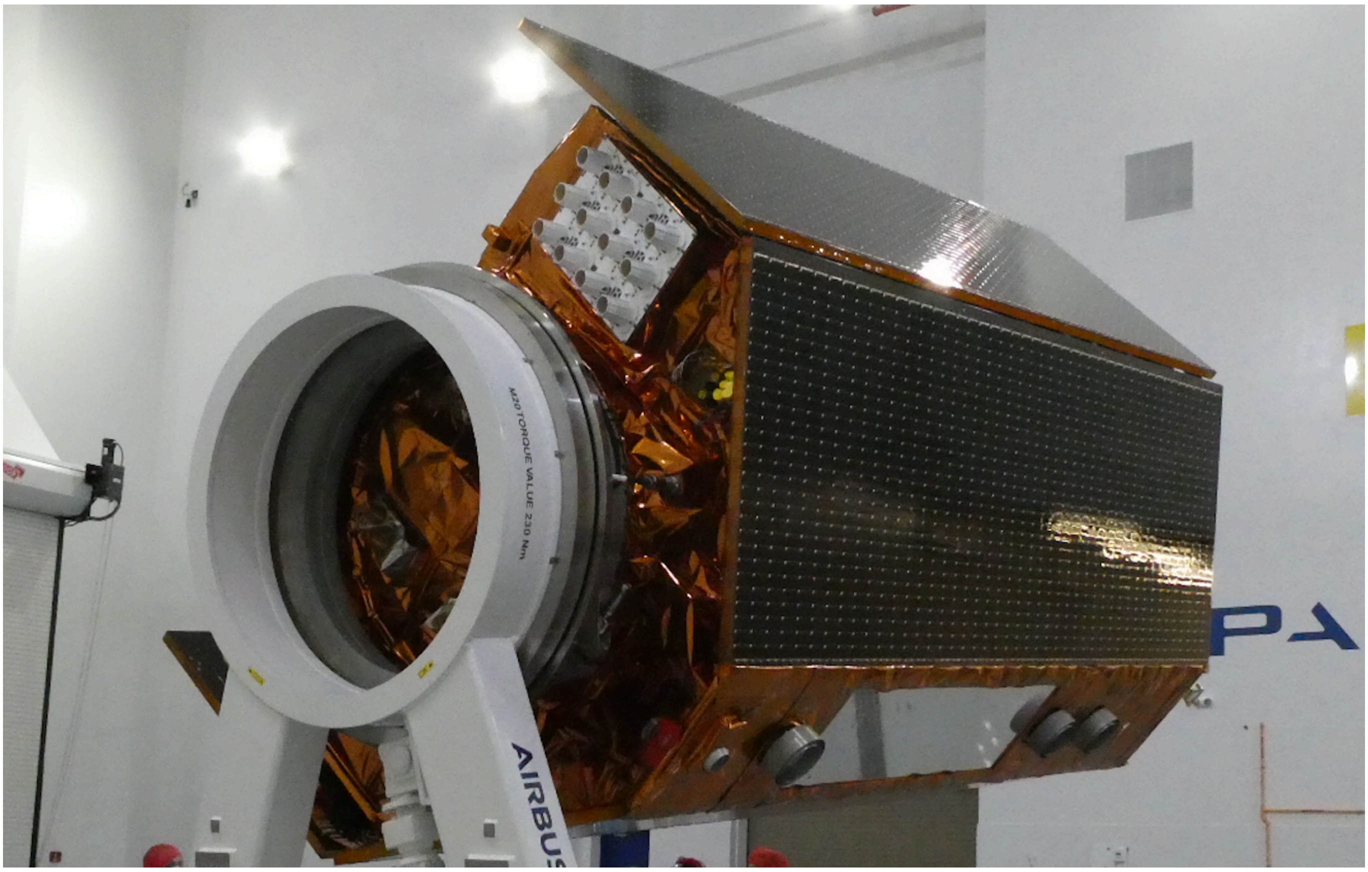

Figure 4-16

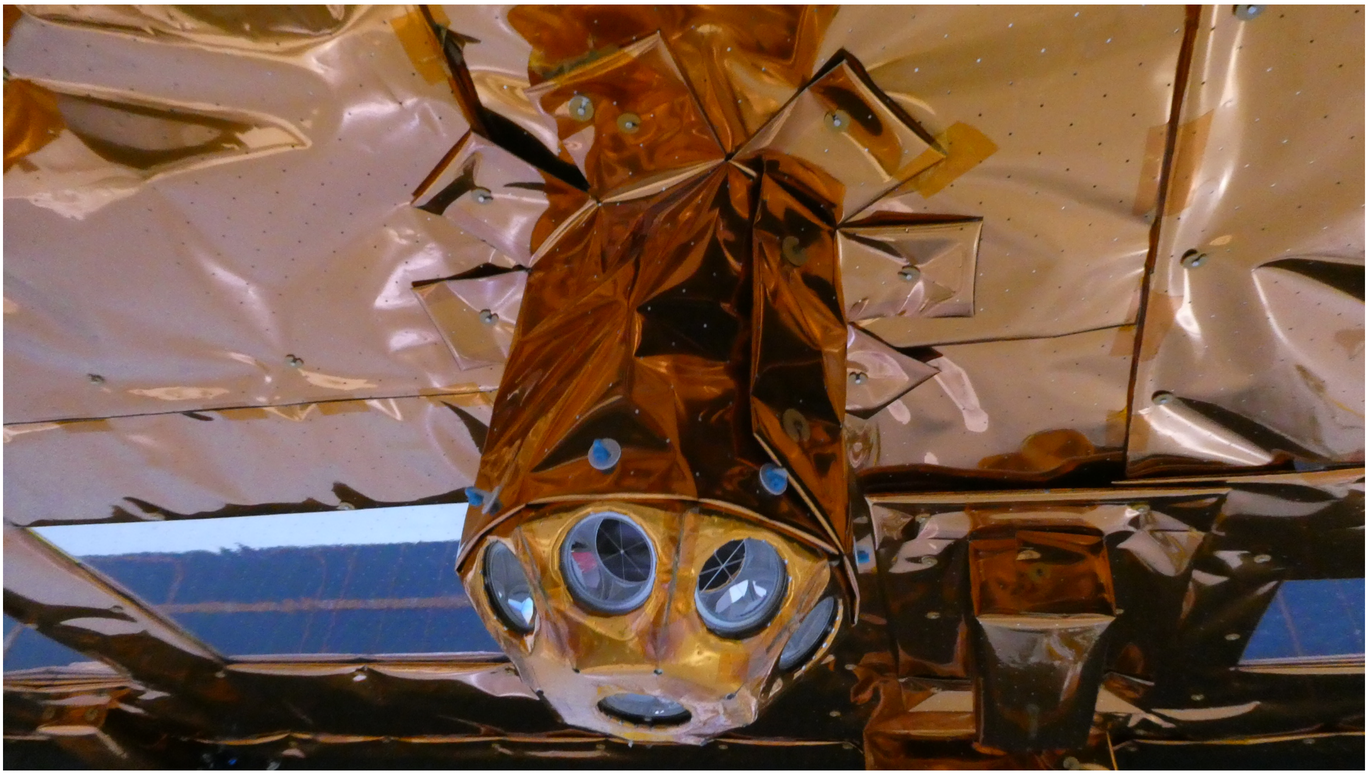

Figure 4-17 Laser Retro-Reflector

Figure 4-18

Figure 4-19